Simulation of seismic attributes for earth models with different continuity properties

Marianne Dagsland Jåsund

THESIS FOR THE DEGREE
MASTER OF SCIENCE

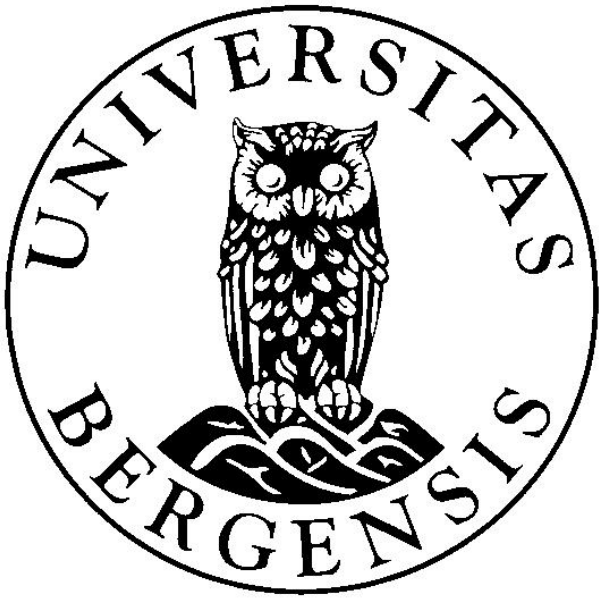

Department of Earth Science

University of Bergen

October 15, 2019

Chapter I

I have never tried that before, so I think I should definitely be able to do that!

- Pippi Longstocking

Abstract

The combination of kinematic and dynamic ray tracing has been used since the 1970s for simulation (modelling) of seismic energy in the subsurface. Kinematic/dynamic ray tracing is used to simulate the travel time, amplitude and wavefront curvature of a seismic wave— these results are typically presented in the form of curves, maps or synthetic seismograms. Kinematic/dynamic ray tracing is known as a flexible and fast method with the advantage of allowing the user to choose which parts of the wavefield to be simulated. For calculation of amplitudes using dynamic ray tracing, the second-order derivatives of the velocity field must be known. As a consequence, the function representing the velocity field must be, as a minimum, C^2 continuous, and this is why cubic splines traditionally has been used. In this study, I test the use of the quintic (fifth degree) B-spline representation. The main objective is to examine whether a quintic B-spline can make kinematic and dynamic ray tracing more robust with respect to local variations in the velocity field. I have done tests of direct ray tracing and two-point ray tracing in the Marmousi model and in a salt model. Both models were exposed to different degrees of smoothing. I compare the results obtained using the cubic and the quintic B-spline representations. For each representation I calculated a number of ray paths, travel times, amplitudes and seismograms, and I monitored the computation times. The results show that for a model with a relatively strong local velocity variation, a quintic representation provides a considerably higher degree of robustness for two-point ray tracing. For models with a higher degree of smoothness, I observe only small differences in the modelling results for the cubic and quintic representations. The quintic B-spline gives increased computation time, but on the other hand a general improvement in robustness.

Chapter III

Acknowledgement

This thesis was written at the Department of Earth Science: Basin and Reservoir Studies (BRS) at the University of Bergen.

First of all, I would like to thank my main supervisor, Einar Iversen, for always having time, and for all guidance and support these past two years. Thank you for being there. A special thanks to my co-supervisor Einar Mæland for teaching me about splines and all that goes with it, you are great! Thanks to NORSAR and MathWorks for the academic licence of NORSAR-3D and MATLAB respectively.

To all the guys at Drivhuset, thanks for all the laughter. A huge thanks to my brother, Rune Jåsund, for proofreading, and to the rest of my family for believing in me.
Finally, to my fiancé, Thomas, thank you for being so patient.

Chapter V

Contents

List of Figures

1 Introduction

Ray methods have been used for many years to study propagation of seismic energy in the subsurface. To start with, the purpose was mainly on calculating ray paths and travel time, this is known as kinematic ray tracing. In the 1970s there was a development of numerical techniques for dynamic ray tracing, by which one may calculate wavefront curvature and geometrical spreading (Červený and Hron, 1980, Gjøystdal et al., 2007, Farra and Madariaga, 1987, Červený, 1972). In the 1980s, primarily as the result of the work by Červený et al. (1982), the interest was expanded beyond dynamic ray tracing to the paraxial ray method (Keho et al., 1987). Since then, extensive work has been done in the field, (Bortfeld, 1989, Červený et al., 1988, Červený, 2001, Klimeš, 2002, Červený et al., 2012, Iversen et al., 2019). Paraxial ray methods allow for approximation of seismic attributes in the near vicinity of a reference ray. The paraxial extrapolation of travel time, and also calculation of the amplitude depends on the second order derivatives of the velocity field. As a minimum, the function representing the velocity field has to be C^2, which means that the function has continuous first and second order derivatives. To fulfil this requirement, cubic B-splines have traditionally been used. The advantage of the B-spline is its local nature, which means that if we change the velocity in a single point in a discrete velocity model, the effect on the function value and its derivatives will only be noticeable in the near vicinity of that point. For stable ray tracing results using cubic B-spline representation, excessive “pre” smoothing of the geological model is often required. By employing higher order spline representation for the velocity, the second order derivatives of velocity become more stable, and there will be a greater smoothing along the ray. Another advantage of the use of the higher order spline representation is the access to stable higher order derivatives needed for higher order extrapolation of travel time.

In this thesis I study the effect of the quintic spline representation on the calculation of seismic attributes. Seismic attributes such as travel time, ray path, and amplitude are calculated using both the cubic and the quintic spline representations, and then compared. The resulting attributes are presented in maps and seismograms. My motivation is to address the potential of using a higher order spline in the representation of geological models.

This thesis is divided into 7 chapters. In chapter 2, I give a brief introduction to forward modelling, ray-based methods and basic splines. In chapter 3, I consider the most important derivations pertaining to kinematic and dynamic ray tracing and explain the method used for B-spline representation. The derivations in this chapter are used to construct the ray tracing codes in Matlab. In chapter 4, I address the smoothing ability of the quintic B-spline, and elaborate on the robustness of two-point ray tracing when using the cubic and the quintic spline representations. The behaviour of ray paths and differences in amplitude are presented in plots and synthetic seismograms. In chapter 5 I discuss the results from chapter 4, and in chapter 6 I give my conclusions and propositions to further work.

2 Background

In this chapter I give a brief introduction to forward modelling, and why it is used. I also introduce the method of forward modelling used in this thesis, the ray tracing method. Here I will discuss briefly what a ray is, why the method is popular and, what attributes that can be extracted. In the last section of this chapter, I introduce the method used for smoothing and representation of velocity— the B-spline method.

2.1 Forward modelling

In the context of this thesis, forward modelling means to simulate a seismic response for a given geological model. This is done by solving the equation of motion for seismic waves. As output, we then get synthetic seismograms, which may be compared to real seismic data. If the synthetic and real data are consistent, the geological model can be taken to be accurate. The opposite of forward modelling is inverse modelling. This is the method of computing a geological model, or an image of the subsurface, from real seismic data (Krebes, 2004). Inverse modelling is referred to as inversion, and from now on, forward modelling will be referred to as just modelling.

Modelling yields the opportunity to study the behaviour of seismic waves in the subsurface by numerical simulations. Modelling may be used in several stages, but there always have to be a general idea of what the survey area looks like. Forward modelling can then be used for survey planning, i.e. to find the survey geometry which best illuminate an area of interest. A common utilization of modelling is to validate the interpretation of seismic data. Modelling can also be used to determine how seismic energy behave near certain geological features, and if it is possible to recognise these directly from seismic data.

There are different methods of modelling that can be used, depending on multiple factors such as time, computational cost, demand for accuracy and resolution. These methods are divided in to three classes: direct methods, integral-equation methods and ray tracing methods (Carcione et al., 2002). Direct methods and integral-equation methods will not be considered in this thesis, but a brief introduction will be given.

Direct methods model the complete wavefield, these methods can be very accurate when a sufficiently fine grid is used, but they require a lot of computational time. Finite difference is an example of direct methods. This can be applied to solve partial differential equations, and in the case of the wave equation, the finite difference method models the complete wavefield. This method provide snapshots of the propagation of the wave and synthetic seismograms (Gjøystdal et al., 2002, Lecomte et al., 2015, Krebes, 2004).

Integral-equation methods are based on Huygen's principle. These are more restrictive than the direct methods and ray tracing methods. For geophysical applications, the integral equation methods are often used in electromagnetic modelling (Zhdanov et al., 2006).

The last class of modelling methods is the ray-tracing methods. These are based on the high frequency approximation of the wave equation and will be discussed in the next section.

2.2 Rays and wavefronts

A *ray* is a mathematical concept for describing a path of energy from its source. Throughout the thesis I use travel time as the variable along the ray. Other choices are possible, e.g., travel distance. A *wavefront* is a surface along which the travel time is constant. This means that to trace a ray corresponds to following a point situated on the moving wavefront. In isotropic media, the ray path is always perpendicular to a this moving wavefront (Červený et al., 1977).

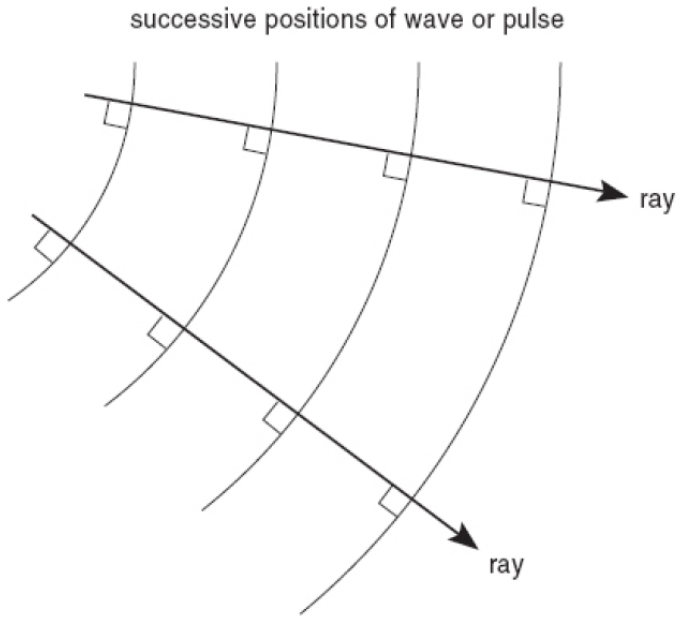

Figure 2.1: *In an isotropic medium the rays are perpendicular to the wavefront. Illustration from (Mussett and Khan, 2000).*

The method of ray tracing is frequently used because it is a very fast, and a cost-efficient method considering the computational time. This is an advantage when working with large 3D models. Another advantage of ray tracing is that it is possible choose which part of the wavefield to model, as opposed to a direct method which provides the complete wavefield. As a result of this, only the reflected ray can be modelled, or refracted ray, multiples can simulated, or excluded. In other words, ray tracing is a very flexible method. (Lecomte et al., 2015)

In general, ray tracing can be divided into kinematic and dynamic ray tracing. From kinematic ray tracing, travel time and ray path can be extracted. Whereas amplitude, geometrical spreading and wavefront curvature can be extracted from dynamic ray tracing (Gjøystdal et al., 2007). The attributes extracted from dynamic ray tracing can be used for paraxial extrapolation of amplitude, geometrical spreading and travel time. Calculation of ray paths falls into two categories: 1) direct ray tracing, where the ray path is found by a given initial condition (for example by the components of the slowness vector at the source point), and 2) two point ray tracing, where a certain boundary condition needs to be fulfilled, typically that the rays should reach a given receiver point. Two-point ray tracing typically needs to be solved iteratively, and information from (direct) dynamic ray tracing may preferably be used for each step in the iterative process.

Ray tracing is a (forward) modelling method. As such, it requires a known geological model, which in its simplest form consist of a smooth, continuous grid of the P-wave velocity and the density of the medium. The model has to be smooth and the model parameters must vary slowly (Gjøystdal et al., 2002). If the model parameters vary too much over the wavelength of the signal, it is not a good model for ray tracing. The ray method is a high frequency method, which imply a small wavelength. If the model parameters vary with a longer wavelength than the dominating wavelength in the seismic signal, the model is suited for ray tracing (Červený, 2001).

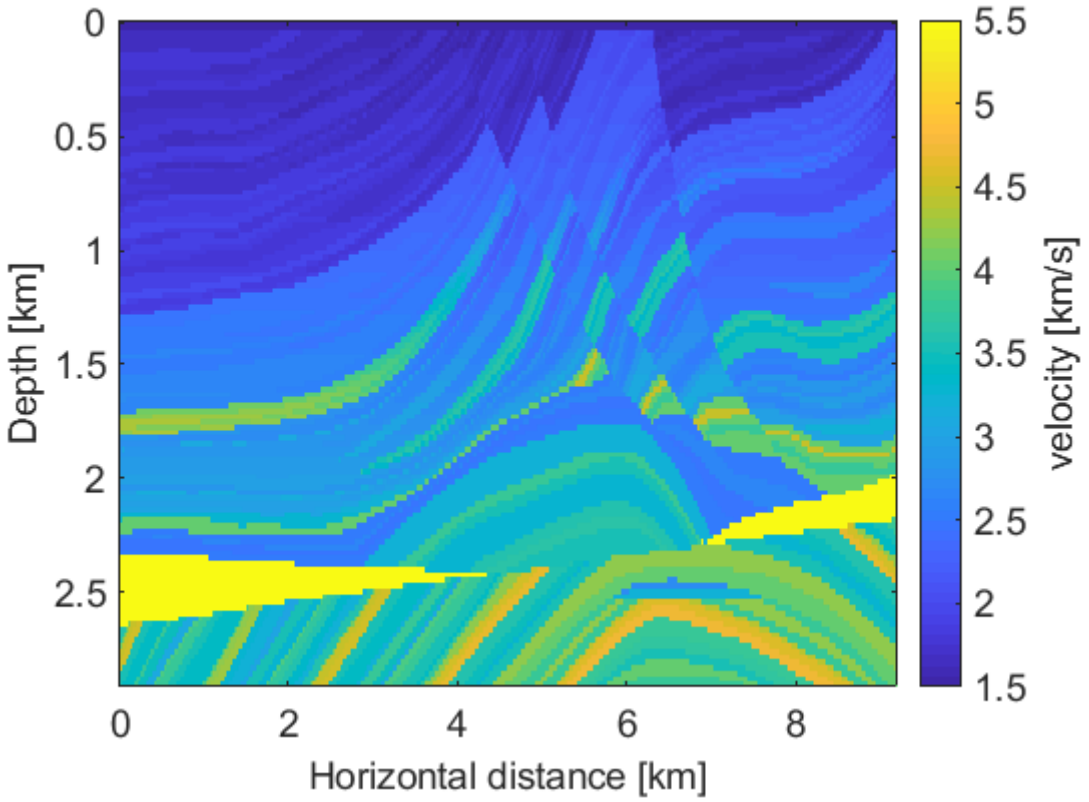

Figure 2.2: *The Marmousi model*

Figure 2.2 yields an example of a model in which ray tracing has difficulties, as a result of numerous discontinuities and rapid changes of the velocity. What is often done for a model such as the Marmousi model is to apply a smoothing "filter". By convolving the model grid points with a positive dimensionless function, with a function value less than one, the magnitude of the velocity in each grid point will decrease. One method for achieving this

effect is the *Basic splines* method.

2.3 Basic splines

In mathematics, a spline is defined as a piecewise polynomial function. The word spline originates from the shipbuilding industry; a wooden beam used to draw smooth curves. The word probably dates back to the 1600's. (Farin et al., 2002).

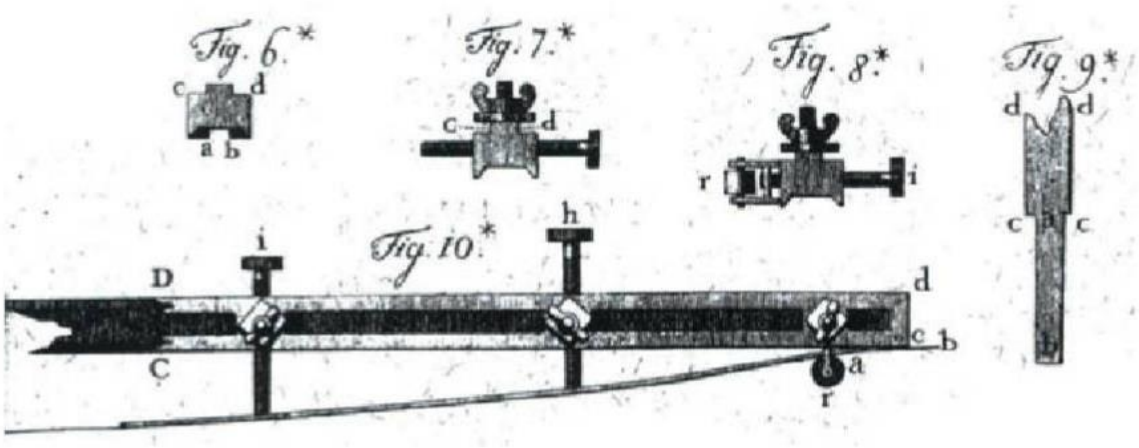

Figure 2.3: *A mechanical spline from the 1700s (Farin et al., 2002).*

B-splines (Basic splines), have been used for several years in Computer Aided Geometric Design (CAGD), and in seismic modelling. It was first introduced in 1946 by Isaac Jacob Schoenberg and was later used as a tool by Carl R. de Boor in General Motors research lab in the 1960s. de Boor has also developed the recursive de Boor algorithm (Farin et al., 2002).

Figure 2.4: *Citroën DS (Ushakov, 2011)*

While B-spline was developed as a tool in curve fitting, a similar method, was developed by Pierre Bezier, see Chang and Sederberg (1997). Bezier worked with curve fitting and developed, parallel with de Boor, the Bezier curve. Bezier curves can be expressed by Bernstein polynomials. These polynomials can be found using the recursive method developed by Paul de Casteljau (at Citroën), the de Casteljau algorithm, see Nowak (2011). Later it was discovered that de Boors recursive B-spline evaluation was a generalisation of the de Casteljau algorithm (Farin et al., 2002).

One advantage of using B-spline is that it has continuous derivatives to n-2 degrees, where n is the order of the spline, and the degree of the spline is N = n-1. The order of the spline is equal to the number spline segments of the spline curve (i.e. the number of B-spline basis functions).

Another advantage of the B-spline is that it is a local method, which means that only a part of the curve, in near vicinity, is affected if one of the control points is altered. The Bezier method, on the other hand, is a global method, which means that a change of one control point affects the whole function.

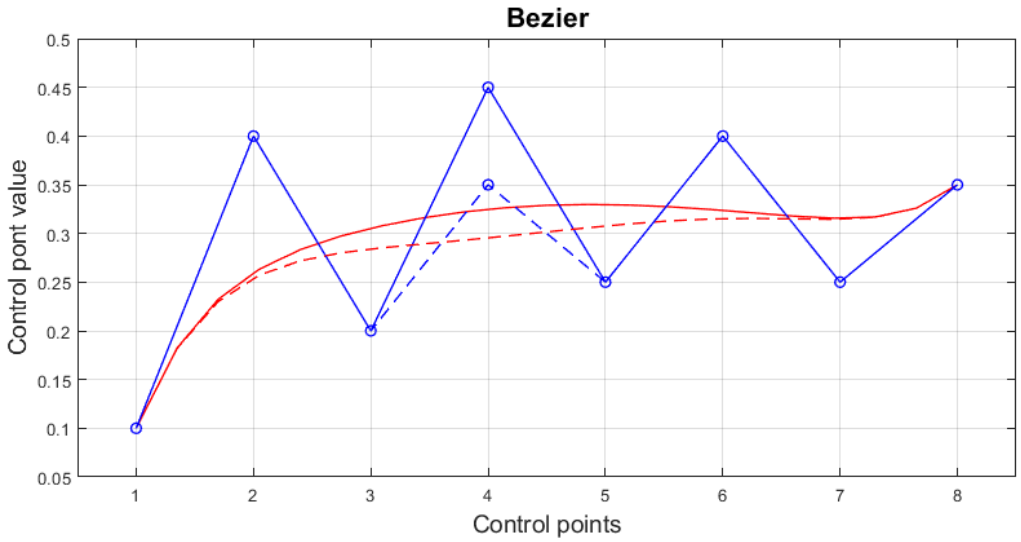

Figure 2.5: *Control point polyline (solid blue) and its corresponding Bezier curve (solid red). The corresponding dashed versions results when one control point is altered.*

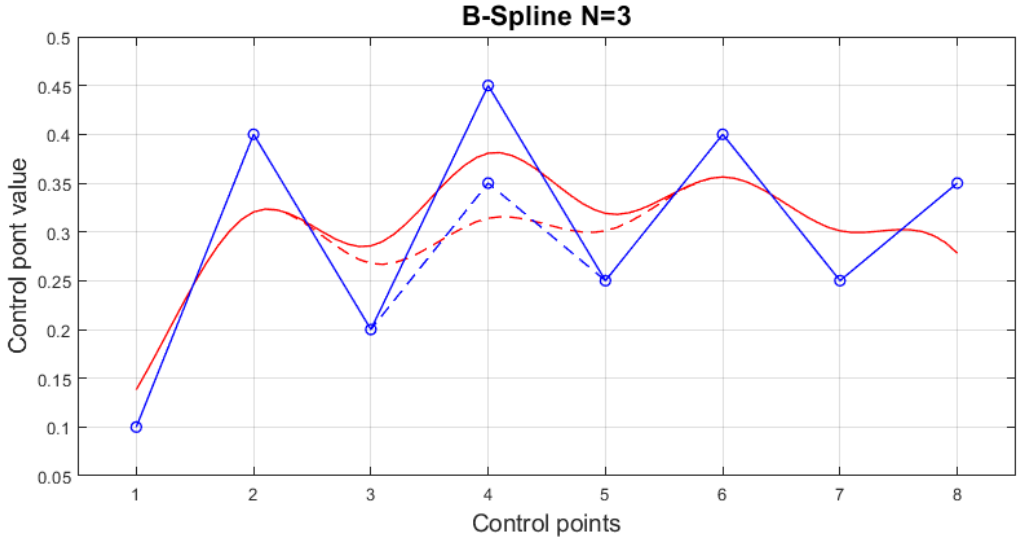

Figure 2.6: *Control point polyline (solid blue) and its corresponding B-spline curve (solid red). The corresponding dashed versions results when one control point is altered.*

Figures 2.5 and 2.6 illustrates how the curves are altered when changing one of the control points. Regarding the portion of curve altered, the Bezier curve is affected to a greater degree than the cubic B-spline curve. The B-spline curve changes locally, whereas the Bezier curve changes globally, i.e. the entire curve is altered (except the endpoints).

Another property of B-splines is how the stiffness of the curve vary with the degree of the spline. The capability to bend decreases as the order of the spline increases.

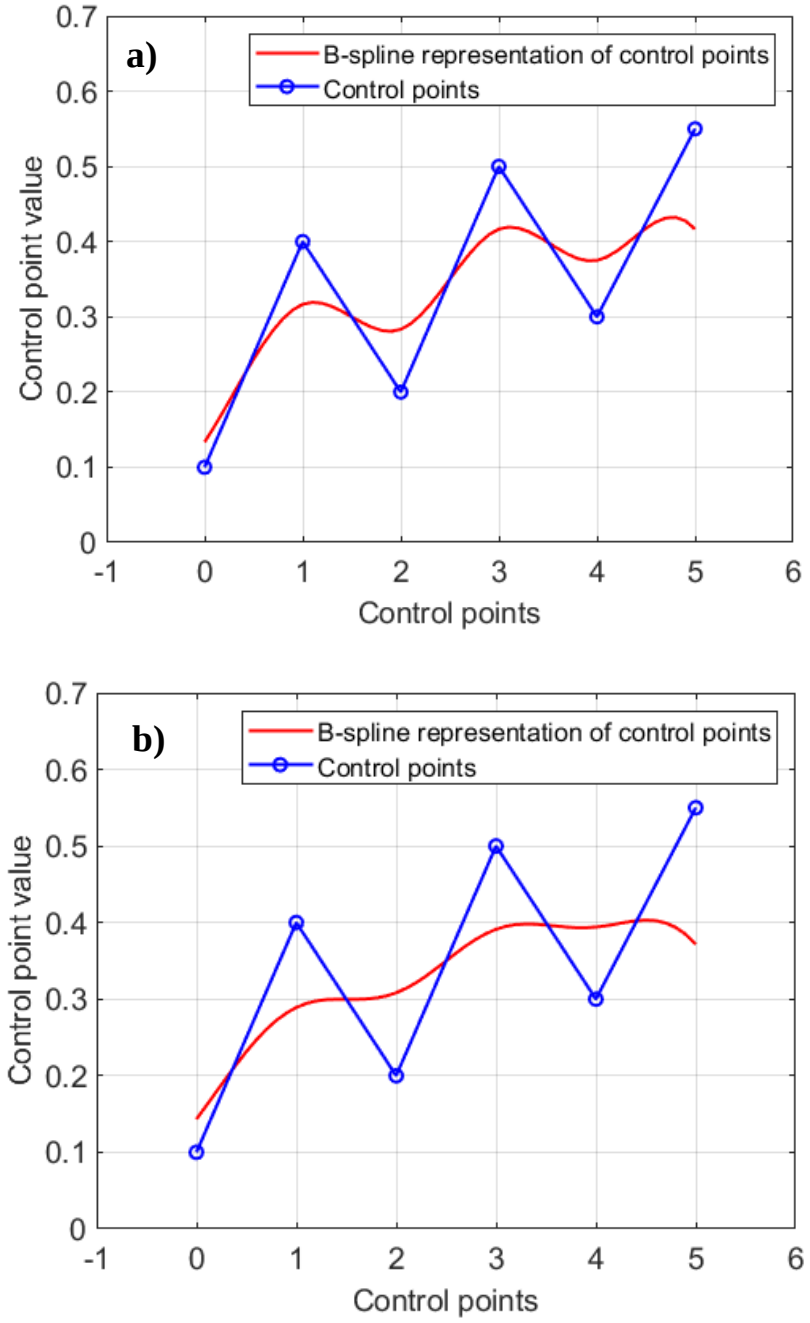

Figure 2.7: *Illustration of the increasing stiffness of higher order splines. a) cubic spline representation of control points, b) quintic spline representation of control points.*

As can be seen from Figure 2.7, the quintic spline representation of the control points are smoother than the cubic spline representation. This will, when employing a quintic spline representation, lead to greater smoothing along the ray while doing ray tracing.

3 Theory/Method

In order to test the effect of quintic spline representation on the seismic attributes, ray tracing needs to be done. The theory presented in this chapter is used to construct Matlab programs for modelling ray path, travel time and amplitude using both direct and two-point ray tracing. How to extrapolate travel time and identify caustics are also discussed

.

3.1 Ray tracing

In this subsection I look at the derivations and numerical methods used in kinematic and dynamic ray tracing. The derivations follow Červený (2001).

The wave equation describes how a wave behaves in the subsurface. When solved without approximations, the wave equation will provide the complete wavefield. Solving the equation for the complete field is a tedious and time-consuming task, but this field might not be needed.

The wave equation can be approximated for high frequencies. This high frequency approximation yields two important equations, the Eikonal equation and the transport equation. For an isotropic medium, the Eikonal equation is on the form

$$(\nabla T)^2 = \frac{1}{c(x,y,z)^2} \tag{3.1}$$

and the transport equation is on the form

$$2\nabla A \cdot \nabla T + A\nabla^2 T = 0 \tag{3.2}$$

where T is the travel time, c is the wave velocity, which only dependends on position, and A is the amplitude. The Eikonal equation is a first order non-linear partial differential equation, that, when solved provides the wavefronts of a wave. The gradient of the travel time (∇T) is equal to the slowness. In seismology it is common with a more general consideration of ray

path, where ray tracing can be described in terms of the Hamilton canonical equations (Drummond, 1982, Keers et al., 1997).

In Hamiltonian form, equation (3.1) can be expressed as

$$\mathcal{H} = \frac{1}{2}(c^2 p_i p_i - 1) \tag{3.3}$$

where p_i denotes the components of the slowness vector, and $\mathcal{H}$ is the Hamiltonian function. The Hamiltonian represents a generalisation of the Eikonal equation. The form of $\mathcal{H}$ depends on whether the medium is isotropic or anisotropic and on the wave mode under consideration. The ray tracing equations for a Hamiltonian approach are

$$\frac{dx_i}{du} = \frac{\partial \mathcal{H}}{\partial p_i} \tag{3.4}$$

$$\frac{dp_i}{du} = -\frac{\partial \mathcal{H}}{\partial x_i} \tag{3.5}$$

where u is some parameter along the trajectory, and x_i is the components of the position vector. This parameter cannot be chosen arbitrary and depends on the specific form of $\mathcal{H}$. In this thesis the variable u is the travel time *t* and the medium is isotropic. Then, the relation, for equation (3.3), $dt/du = p_i \, \partial \mathcal{H}/\partial p_i = 1$ is satisfied.

The derivations presented in the following are valid for both isotropic and anisotropic media.

In ray tracing the purpose is to find the path of seismic (energy) propagation, and the time it takes from a source to a given position. This means we need to calculate position and direction as a function of time or distance. The kinematic ray equations can be expressed as first order derivatives of (3.3):

$$\frac{dx_i}{dt} = \frac{\partial \mathcal{H}}{\partial p_i} \tag{3.6}$$

$$\frac{dp_i}{dt} = -\frac{\partial \mathcal{H}}{\partial x_i} \tag{3.7}$$

Equations (3.6-3.7) give the derivatives of position and slowness with respect to time. When solved, they provide the position and slowness vectors as a function of travel time along the ray.

Attributes such as amplitude, geometrical spreading and curvature of the wavefront, are found by dynamic ray tracing. In the latter, we compute matrix quantities **Q** and **P**, with the components

$$Q_{iA} = \frac{\partial x_i}{\partial \gamma_A}, \tag{3.8}$$

$$P_{iA} = \frac{\partial p_i}{\partial \gamma_A}. \tag{3.9}$$

The quantities **Q** and **P** include the effect of a slight change of a set of initial parameters $\boldsymbol{\gamma} = (\gamma_A)$ (e.g. angles or position components), at a predesignated point (**x**) on the ray. This provides information about rays in the vicinity of the reference ray. Additionally, matrices **Q** and **P** provide information about the curvature of the wavefront, geometrical spreading and amplitude. Matrix **Q** yields the change in position **x** with respect the initial parameter, $\boldsymbol{\gamma}$. Matrix **P** yields the change in slowness with respect to the same parameters. In equations (3.6-3.7) we can use that the differential operators $\partial/\partial\gamma_A$ and d/dt commutes. For the situation with two initial parameters we then get 12 differential equations:

$$\frac{dQ_{iA}}{dt} = A_{ij}Q_{jA} + B_{ij}P_{jA} \tag{3.10}$$

$$\frac{dP_{iA}}{dt} = -C_{ij}Q_{jA} - D_{ij}P_{jA} \tag{3.11}$$

The 12 differential equations from (3.10) and (3.11) can be expressed in a matrix system:

$$\begin{bmatrix} \frac{d\boldsymbol{Q}}{dt} \\ \frac{d\boldsymbol{P}}{dt} \end{bmatrix} = \begin{bmatrix} \boldsymbol{A} & \boldsymbol{B} \\ -\boldsymbol{C} & -\boldsymbol{D} \end{bmatrix} \begin{bmatrix} \boldsymbol{Q} \\ \boldsymbol{P} \end{bmatrix}, \tag{3.12}$$

where $d\boldsymbol{Q}/dt$,$d\boldsymbol{P}/dt$, $\boldsymbol{Q}$ and $\boldsymbol{P}$ are 3 x 2 matrices, and $\boldsymbol{A}$, $\boldsymbol{B}$, $\boldsymbol{C}$ and $\boldsymbol{D}$ are 3 x 3 matrices. The matrices $\boldsymbol{A}$, $\boldsymbol{B}$, $\boldsymbol{C}$ and $\boldsymbol{D}$ represent the second order partial derivatives of the Hamiltonian:

$$A_{ij} = \frac{\partial^2 \mathcal{H}}{\partial p_i \partial x_j}, \tag{3.13}$$

$$B_{ij} = \frac{\partial^2 \mathcal{H}}{\partial p_i \partial p_j}, \tag{3.14}$$

$$C_{ij} = \frac{\partial^2 \mathcal{H}}{\partial x_i \partial x_j}, \tag{3.15}$$

$$D_{ij} = \frac{\partial^2 \mathcal{H}}{\partial x_i \partial p_j}. \tag{3.16}$$

Equations (3.6-3.7) and (3.10-3.11) are general expressions for the kinematic and dynamic ray tracing equation, respectively. For isotropic media the Eikonal equation is on the form (3.1).

3.1.1 Isotropic case

In this subsection, only the isotopic case is considered. Equations (3.6-3.7) and equations (3.13-3.16) for isotropic media then becomes:

$$\frac{dx_i}{dt} = c^2(\boldsymbol{x})p_{\mathrm{i}} \tag{3.17}$$

$$\frac{dp_{\mathrm{i}}}{dt} = -\frac{1}{c(\boldsymbol{x})}\frac{dc(\boldsymbol{x})}{dx_i} \tag{3.18}$$

$$A_{ij} = 2c\frac{dc}{dx_j}p_i \tag{3.19}$$

$$B_{ij} = \delta_{ij}c^2 \tag{3.20}$$

$$C_{ij} = \frac{dc}{dx_i}\frac{dc}{dx_j} + \frac{\partial^2 c}{\partial x_i \partial x_j}\frac{1}{c^2} \tag{3.21}$$

$$D_{ij} = 2c\frac{dc}{dx_i}p_j \tag{3.22}$$

As can be seen from equation (3.21) , the second order derivatives of the velocity needs to be known. For calculation of amplitudes, that depends on the quantities found from dynamic ray tracing, the second order derivatives are required to be continuous. This means that representation of the medium has to be C^2, and is also the reason why cubic splines traditionally have been used to represent velocity in ray tracing models.

3.1.3 Numerical solution

There are several numerical methods for solving differential equations. An ordinary differential equation (ODE) is defined on the form,

$$\frac{d\omega}{dt} = f(t, \omega), \tag{3.23}$$

where $f(t, \omega)$ is known. Euler's method is a simple way of solving ODE's, this is an easy and fast method, but it has relatively large errors. A more reliable approach is the fourth order Runge Kutta method.

Equations (3.6-3.7) and equations (3.10-3.11) are solved numerically with the fourth order Runge Kutta method. The basic formula in the fourth order Runge Kutta method is given by Sauer (2012)

$$\omega_{i+1} = \omega_i + \frac{h}{6}(S_1 + 2S_2 + 2S_3 + S_4), \tag{3.24}$$

where h is the step length, ω_i is the initial value, for $i = 0$, $\omega_0 = \omega(t_0)$, and ω_{i+1} is the value after $i+1$ steps. The quantities S_1, S_2, S_3 and S_4 are given by

$$S_1 = f(t_i, \omega_i),$$

$$S_2 = f(t_i + \frac{h}{2}, \omega_i + \frac{h}{2}S_1),$$

$$S_3 = f(t_i + \frac{h}{2}, \omega_i + \frac{h}{2}S_2),$$

$$S_4 = f(t_i + h, \omega_i + hS_3).$$

The increment based on the slope at the beginning of the interval h is S_1. Increment S_2 and S_3 evaluates the slope at the midpoint of the interval, and S_4 evaluates the slope at the end of the interval. This means that the function is evaluated at four places on the interval [0, h].

Before solving the differential equations, the initial values must be known. For equation (3.6) and equation (3.7), the initial value is the velocity in the source position. The initial value for slowness in the source, is found from the velocity in the source. This is because the norm of the slowness vector is equal to the inverse of the velocity. For a point source, as is used in this study, there is no change in position when travel time is equal to zero, therefor the initial value of matrix **Q** is zero.

The initial value for matrix **P** is found by:

$$P_{\mathrm{iM}} = [\delta_{ij} - p_i p_j]\varepsilon_{jM} = \alpha_{ij}\varepsilon_{jM}\,, \tag{3.25}$$

where $P_{\mathrm{iM}}$is the initial value components of matrix **P,** p_i is the components of the slowness vector in the source and δ_{ij} is the components of the identity matrix. The 3x2 matrix $\boldsymbol{\varepsilon}$ consists of the two unit-vectors, $\boldsymbol{e}_1$ and $\boldsymbol{e}_2$;

$$\boldsymbol{e}_1 = \frac{\hat{\boldsymbol{p}} \times \hat{\boldsymbol{y}}}{\|\hat{\boldsymbol{p}} \times \hat{\boldsymbol{y}}\|},$$

$$\boldsymbol{e}_2 = \hat{\boldsymbol{p}} \times \boldsymbol{e}_1 .$$

These two vectors are orthogonal to the slowness vector $\boldsymbol{p}$. Vector $\hat{\boldsymbol{p}}$ is the normalized slowness vector and $\hat{\boldsymbol{y}}$ is the unit vector in y-direction. Vector $\boldsymbol{e}_2$ is a unit vector orthogonal to the slowness vector and vector $\boldsymbol{e}_1$.

3.2 Two-point ray tracing

Forward modelling may be used to simulate a seismic acquisition, hence, only rays reaching a receiver is of interest. A method to ensure that this happens is two-point ray tracing. A well-known method of two-point ray tracing is the Newton method;

$$\boldsymbol{r}_{rec} - \boldsymbol{r}_{old} = \boldsymbol{\mathcal{B}}\Delta\boldsymbol{\gamma} \tag{3.26}$$

where $\boldsymbol{r}_{old}$ is the coordinates of the endpoint of the initial ray, and $\boldsymbol{r}_{rec}$ is the coordinates of the receiver. The difference in ray parameters in the source position is denoted as $\Delta\gamma$, and $\boldsymbol{\mathcal{B}}$ is the geometric spreading matrix;

$$\boldsymbol{\mathcal{B}} = \left[\frac{d\boldsymbol{r}}{d\gamma_1}, \frac{d\boldsymbol{r}}{d\gamma_2}, \frac{d\boldsymbol{r}}{dt}\right].$$

Here, $d\boldsymbol{r}$ is the change in the endpoint position of the ray due to $d\gamma_A$, the perturbation of ray parameters in the source. The calculations are done in a local coordinate system where the normalized slowness $\hat{\boldsymbol{p}}$ represent the z axis.

3.3 Extracting attributes

There are, as mentioned in section 2.2, several attributes that can be extracted from ray tracing. Travel time, slowness and ray path are calculated directly, while some extra work is required for the computation of amplitudes, geometrical spreading and second order time derivatives. The derivations in this sub section follow Červený (2001).

For the computation of amplitudes, the relative geometrical spreading must be known. Relative geometrical spreading is found by first extending the 3 x 2 matrix $\boldsymbol{Q}$ to the 3 x 3 matrix $\widehat{\boldsymbol{Q}}$:

$$\widehat{\boldsymbol{Q}} = \left[\frac{dx_i}{d\gamma_1}, \frac{dx_i}{d\gamma_2}, \frac{dx_i}{dt}\right] \tag{3.27}$$

The relative geometric spreading is:

$$\mathcal{L}(R,S) = \left|\frac{1}{c(R)}\, det(\widehat{\boldsymbol{Q}}(R))\right|^{1/2} \tag{3.28}$$

and the equation for the amplitude is:

$$U = \frac{1}{4\pi[c(S)c(R)\rho(S)\rho(R)]^{1/2}\,\mathcal{L}(R,S)} \tag{3.29}$$

Equation (3.29) does not consider interfaces or caustics. Here, *U* is the amplitude at a point *R*, *S* is the source position, and *R* is a point on the ray not equal *S*. The velocity in the source position is *c(S)*, *c(R)* is the velocity in point *R* on the ray, *ρ(S)* is the density in the source and *ρ(R)* is the density in point *R* on the ray.

For identification of caustics along the rays, the Keller–Maslov–Arnold-Hörmander (KMAH) index is used (Priimenko and Mitrofanov, 2018). The KMAH index is used to decide the phase of the amplitude in a point on the ray. Caustics along the ray results in a phase shift. There are two types of caustics considered, first order caustics and second order caustics. In the KMAH index, first order caustics are counted as one and second order caustics are

counted as two. The caustic points are found by using the 3x3 matrix $\widehat{\boldsymbol{Q}}$ along the ray. For first order caustics this is done easily by looking at the sign of the determinant of the geometrical spreading matrix. Consider a ray segment with the endpoints P_1 and P_2, and the corresponding matrices $\widehat{\boldsymbol{Q}}_1$ and $\widehat{\boldsymbol{Q}}_2$. From these 3 x 3 matrices, given in cartesian coordinates we can compute the corresponding 2 x 2 matrices $\boldsymbol{Q}_1$ and $\boldsymbol{Q}_2$ given in ray centred coordinates (Červený, 2001).

If

$$det(\boldsymbol{Q}_1)\, det(\boldsymbol{Q}_2) < 0, \tag{3.30}$$

there is a first order caustic between point P_1 and P_2 on the ray, and the number one is added to the KMAH index. Second order caustics are found by checking if

$$tr[\boldsymbol{Q}_1\,(\boldsymbol{Q}_2)^{-1}]det(\boldsymbol{Q}_1)\, det(\boldsymbol{Q}_2) < 0. \tag{3.31}$$

If equation (3.31) holds, there is a second order caustic between the points P_1 and P_2 and the number two is added to the KMAH index.

The phase of the amplitude is found by multiplying U with $e^{iT^c(R,S)}$ where

$$T^c(R,S) = \pm\frac{1}{2}\pi k(R,S) \tag{3.32}$$

Here *k(R,S)* is the KMAH index for a ray between a source *S* and a point on the ray *R*, not equal to *S*.

The extrapolation of travel time depends on the second order time derivatives. These can be found by first extending matrix $\boldsymbol{P}$ to the 3 x 3 matrix $\widehat{\boldsymbol{P}}$;

$$\widehat{\boldsymbol{P}} = \left[\frac{dp_i}{d\gamma_1}, \frac{dp_i}{d\gamma_2}, \frac{dp_i}{dt}\right] \tag{3.33}$$

The 3 x 3 matrix containing the second order time derivatives $\partial^2 T/\partial x_i \partial x_j$ is then

$$\boldsymbol{M} = \widehat{\boldsymbol{P}}\widehat{\boldsymbol{Q}}^{-1} \tag{3.34}$$

The matrix **M** can now be used to estimate travel time for nearby receivers. First, we consider the travel time for a receiver at the location $\mathbf{x_0}$, T($\mathbf{x_0}$). We want to estimate travel time for receivers positioned at coordinates $\mathbf{x_0}+\Delta\mathbf{x}$, so that we find T($\mathbf{x_0}+\Delta\mathbf{x}$). We start by doing a second order Taylor expansion:

$$T(\boldsymbol{x}_0 + \Delta\boldsymbol{x}) = T(\boldsymbol{x}_0) + \frac{\partial T(\boldsymbol{x}_0)}{\partial x_i}\Delta x_i + \frac{1}{2}\left(\frac{\partial^2 T(\boldsymbol{x}_0)}{\partial x_i \partial x_j}\right)\Delta x_i \Delta x_j \tag{3.35}$$

The first order derivative of travel time $\partial T(\boldsymbol{x}_0)/\partial x_i$ is equal to the slowness vector $\boldsymbol{p}$, and the second order derivative of travel time is matrix **M**. Equation (3.35) can then be written in vector notation as:

$$T(\boldsymbol{x}_0 + \Delta\boldsymbol{x}) = T_0 + \boldsymbol{p}_0{}^T\Delta\boldsymbol{x} + \frac{1}{2}\Delta\boldsymbol{x}^T\boldsymbol{M}\Delta\boldsymbol{x} \tag{3.36}$$

$$T^2(\boldsymbol{x}_0 + \Delta\boldsymbol{x}) = (T_0 + \boldsymbol{p}_0{}^T\Delta\boldsymbol{x})^2 + T_0\Delta\boldsymbol{x}^T\boldsymbol{M}\Delta\boldsymbol{x} \tag{3.37}$$

Equations (3.36) and (3.37) are used to calculate paraxial travel time. By that we mean to estimate travel time in the vicinity of a reference ray without the need of additional ray tracing. In a smooth medium, free of caustics, it will be possible to estimate a fairly good representations of the travel time. Equation (3.37) represent the hyperbolic representation of travel time and will, for a point source in an isotropic homogeneous medium, be exact (Iversen et al., 2019). The slowness vector $\boldsymbol{p}$ gives the direction normal to the wavefront, and the matrix $\boldsymbol{M}$ is related to the curvature of the wavefront in position $\mathbf{x}_0$. Matrix **M** is dependent on the second order derivatives of the velocity, which means that extrapolation of travel time requires the representation of the medium being C^2.

3.4 B-spline numerics

As mentioned in section 3.2, cubic splines are needed to represent the velocity model in order to obtain C^2 continuity. In this thesis, B-splines are used to represent the model velocity along a ray. Both third degree (cubic) and fifth degree (quintic) B-splines are used. The theory behind both are the same, and the following illustrations are of cubic splines. A B-spline curve of order k consist of k polynomial pieces of degree N=k-1 (de Boor, 1993). The integral of a B-spline function, of any order, is equal to one.

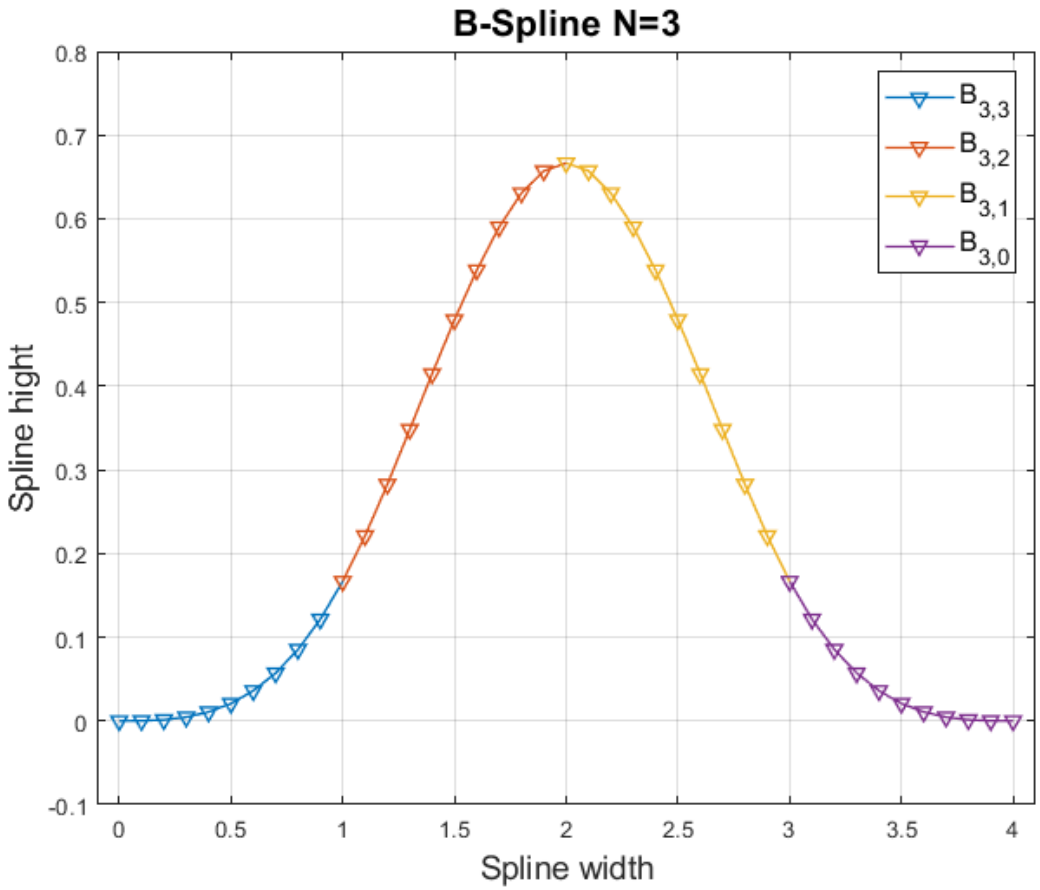

Figure 3.1: *B-spline curve of order 4, presented by its constituent parts.*

Figure 3.1 shows a B-spline curve of order k=4, the degree of the fourth order polynomials are then of third degree. These polynomial functions are called the basis functions for B-spline of order k. The polynomials are each defined on an interval of length 1. Figure 3.2 illustrates the basis functions on the interval [0,1].

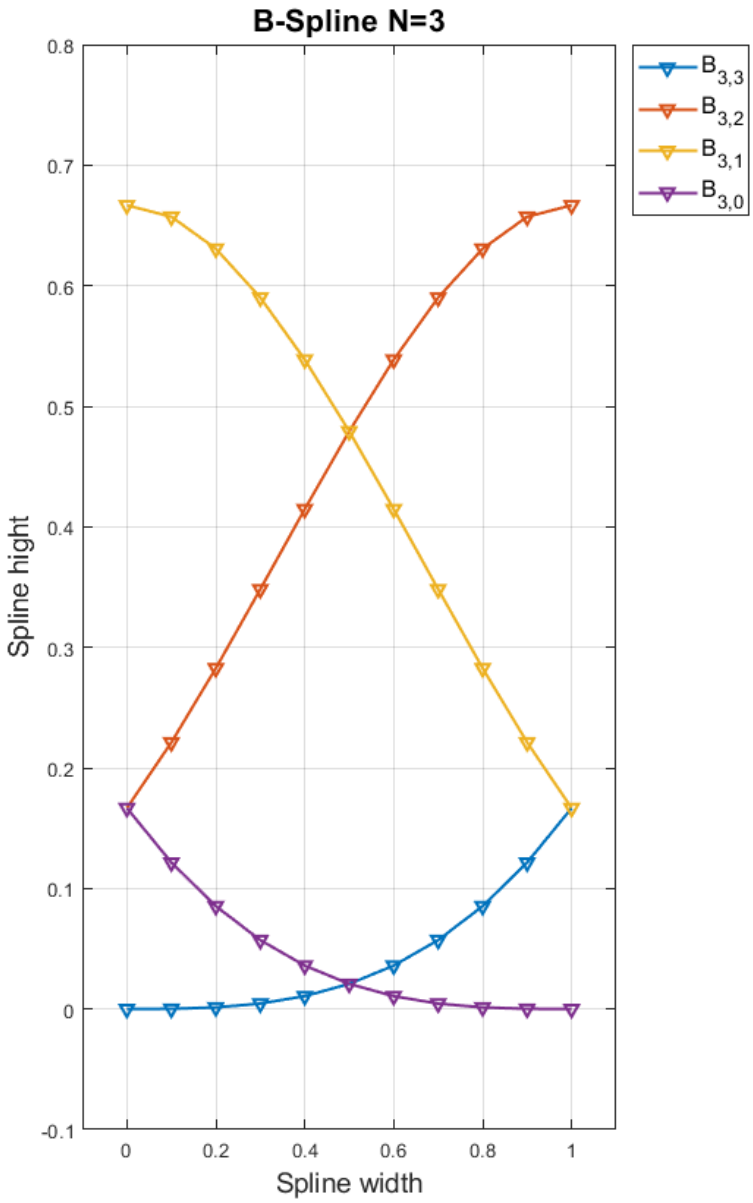

Figure 3.2: *The B-spline segments of the fourth order B-spline function defined on the interval [0,1].*

The basis functions for the polynomials are found from the recursive de Boor function (de Boor, 1978):

$$B_{i,k} = B_{i,k-1}(t)\frac{t - t_i}{t_{i+k-1} - t_i} + B_{i+1,k-1}(t)\frac{t_{i+k} - t}{t_{i+k} - t_{i+1}} \tag{3.38}$$

Equation (3.37) is valid for both varying and equidistant intervals. Here $B_{i,k}$ is the basis function for a polynomial of order *k*, where *i* is the associated control point index and *t* represent the independent variable. For first order B-spline (k=1), the basis function is equal to one for $i=i_0$, where i_0 is the index of a selected control point. For any other recursion step, $B_{i,k} = 0$, if $i > i_0$. For further information see de Boor (1978).

When representing a set of control points by a curve, the B-spline function is convolved with these control points. The curve will not necessarily go through the points but will be as near as possible. By not forcing a curve through the points, unwanted oscillations may be avoided. The "stiffness" of the curve depends on the order of the spline. As the order of the spline increases, the "stiffness" of the curve will increase.

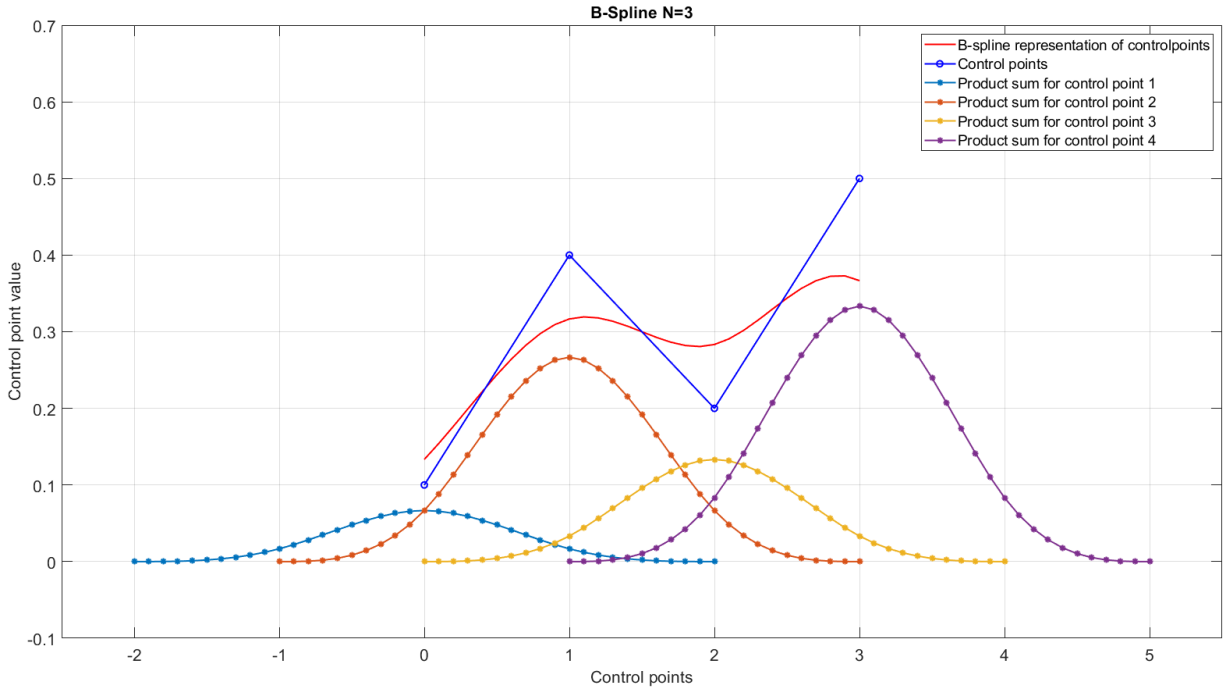

Figure 3.3: *Illustration of the convolution steps representing the control point (blue polyline) by a cubic B-spline spline (red curve). The sum of the B-spline basis functions (coloured dotted curves) equals the cubic B-spline (red curve).*

Figure 3.3 illustrates the B-spline curve (red) for the control points (blue), as a third degree spline function is convolved with the control points.

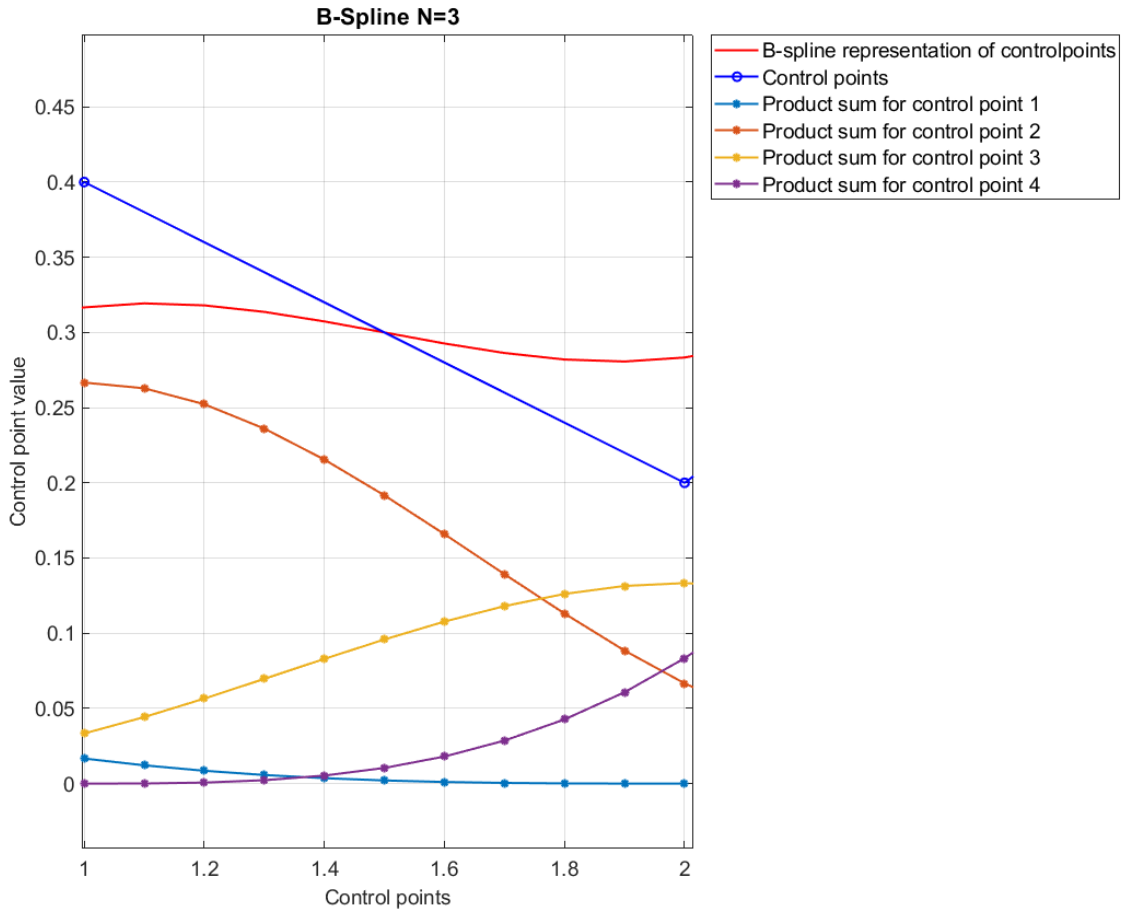

Figure 3.4: *Close up of Figure 3.3 illustrating the spline segments contributing to the B-spline curve between control point 1 and 2.*

When the purpose is to represent only one value, and not the entire curve, the principle of convolution is used in a different way. Figure 3.4 shows the pieces of the curves from Figure 3.3 that contributes to the B-spline curve between control points 1 and 2. These pieces are the four polynomials that the spline curve consist of, that can be expressed by the B-spline basic functions. From the figure and the rules of convolution it is shown that, on the interval between control point 1 and 2, the red curve equals the sum of the B-spline curve segments.

For a cubic spline representation in 1D, we need two control points on each side of the query point, whereas a quintic representation requires three. One point for each spline segment.

The function for representing a value using B-spline is very similar to discrete convolution. In 1D,

$$M(x) = \mathcal{M}(u) = \sum_{r=r_{min}}^{r=r_{max}} b_r(u) M^r \tag{3.39}$$

where $\mathcal{M}(u)$ and *M(x)* is the represented value for a query point at *x*, where *u* is the scaled value of *x* on the interval [0,1]. The B-spline basic function $b_r(u)$ is defined on the interval (0,1), as illustrated in Figure 3.2. In this thesis I use that $[b_0\ b_1\ b_2\ b_3] = [B_{03}\ B_{13}\ B_{23}\ B_{33}]$. M^r is the value of control point *r* where *r* is the control point number.

In 3D:

$$M(x,y,z) = \mathcal{M}(u,v,\omega) = \sum_{t=t_{min}}^{t=t_{max}} b_t(\omega) \sum_{s=s_{min}}^{s=s_{max}} b_s(v) \sum_{r=r_{min}}^{r=r_{max}} b_r(u) M^{r,s,t} \tag{3.40}$$

As the second order derivative of velocity is also needed, the derivatives of the B-spline representation method are required. We employ the chain rule;

$$\frac{dy}{dx} = \frac{dy}{du}\frac{du}{dx},$$

on equation 3.39 and get:

$$\frac{dM(x)}{dx} = \frac{1}{\Delta x} \sum_{r=r_{min}}^{r=r_{max}} \frac{db_r(u)}{du} M^r \tag{3.41}$$

In 3D, there are three expressions for the partial derivatives with respect to x, y, and z, the partial derivative with respect to x is:

$$\frac{\partial M(x,y,z)}{\partial x} = \frac{1}{\Delta x} \sum_{t=t_{min}}^{t=t_{max}} b_t(\omega) \sum_{s=s_{min}}^{s=s_{max}} b_s(v) \sum_{r=r_{min}}^{r=r_{max}} \frac{db_r(u)}{du} M^{r,s,t} \tag{3.42}$$

For the second order partial derivatives, there are 6 equations, presented below are $\partial^2 M(x,y,z)/\partial x^2$ and $\partial^2 M(x,y,z)/\partial x \partial z$.

$$\frac{\partial^2 M(x,y,z)}{\partial x^2} = \frac{1}{\Delta x^2} \sum_{t=t_{min}}^{t=t_{max}} b_t(\omega) \sum_{s=s_{min}}^{s=s_{max}} b_s(v) \sum_{r=r_{min}}^{r=r_{max}} \frac{d^2 b_r(u)}{du^2} M^{r,s,t} \tag{3.43}$$

$$\frac{\partial^2 M(x,y,z)}{\partial x \partial y} = \frac{1}{\Delta x \Delta y} \sum_{t=t_{min}}^{t=t_{max}} b_t(\omega) \sum_{s=s_{min}}^{s=s_{max}} \frac{db_s(v)}{dv} \sum_{r=r_{min}}^{r=r_{max}} \frac{db_r(u)}{du} M^{r,s,t} \tag{3.44}$$

Figure 3.5 illustrates the derivatives of the cubic spline up to third order. As can be seen, the second order derivative is continuous, which yields C^2 representation of a velocity model.

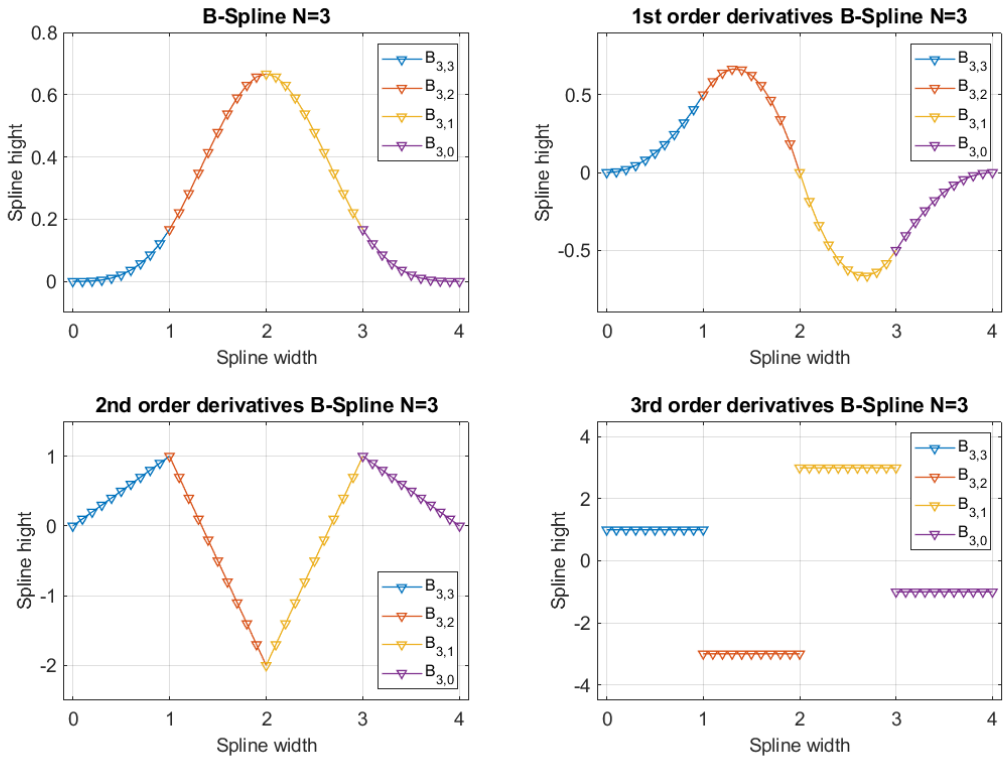

Figure 3.5: *Illustration of the derivatives of a cubic spline curve.*

3.5 Models

The two 3D velocity models used in this thesis was made and prepared in NORSAR-3D. The first model, the Marmousi model, was exported from Matlab as a tigress ascii file in and then imported into NORSAR-3D. There, the model was smoothed to be appropriate for ray tracing. The model was smoothed using a hamming radius of 0.4 km for the first model and 0.3 km for the second model. The Marmousi model has a width of 9.192 km, a depth of 2.904 km and a grid spacing of 0.024 km.

Ray tracing was done in the smoothed Marmousi models and the initial values and the endpoint values of the rays were exported from NORSAR-3D to Matlab. The exported attributes were the slowness vectors at the source and at the receivers, the source coordinates, the receiver coordinates and the travel time.

The second velocity model was made completely in NORSAR-3D. This model is a simple salt model, consisting of two constant velocity parts. The salt model was smoothed to an appropriate degree for ray tracing, using a hamming radius of 0.3 km. The salt model has a

width of 10 km in both x-direction and y-direction, a depth of 5 km and a grid spacing of 0.05 km.

Both models were exported from NORSAR-3D as segy files and imported to Matlab. In Matlab some modifications were done in terms of the smoothness and grid spacing, this is specified in the result chapter for the tests concerned.

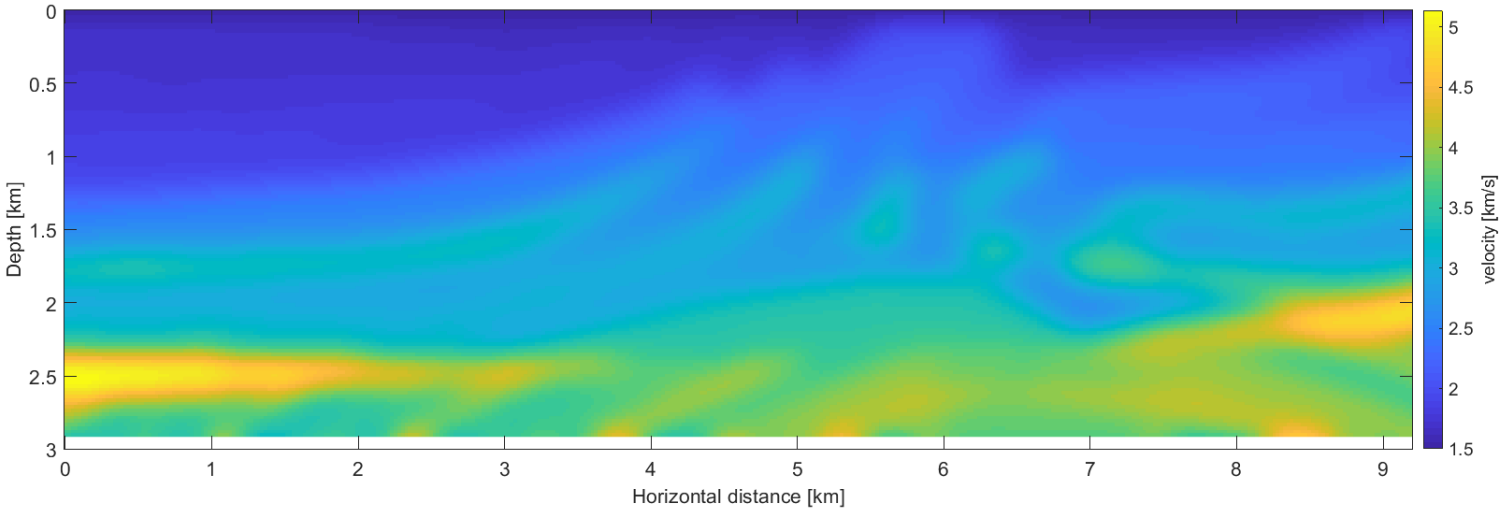

Figure 3.6: *The Marmousi model smoothed with a Hamming radius of 0.4 km.*

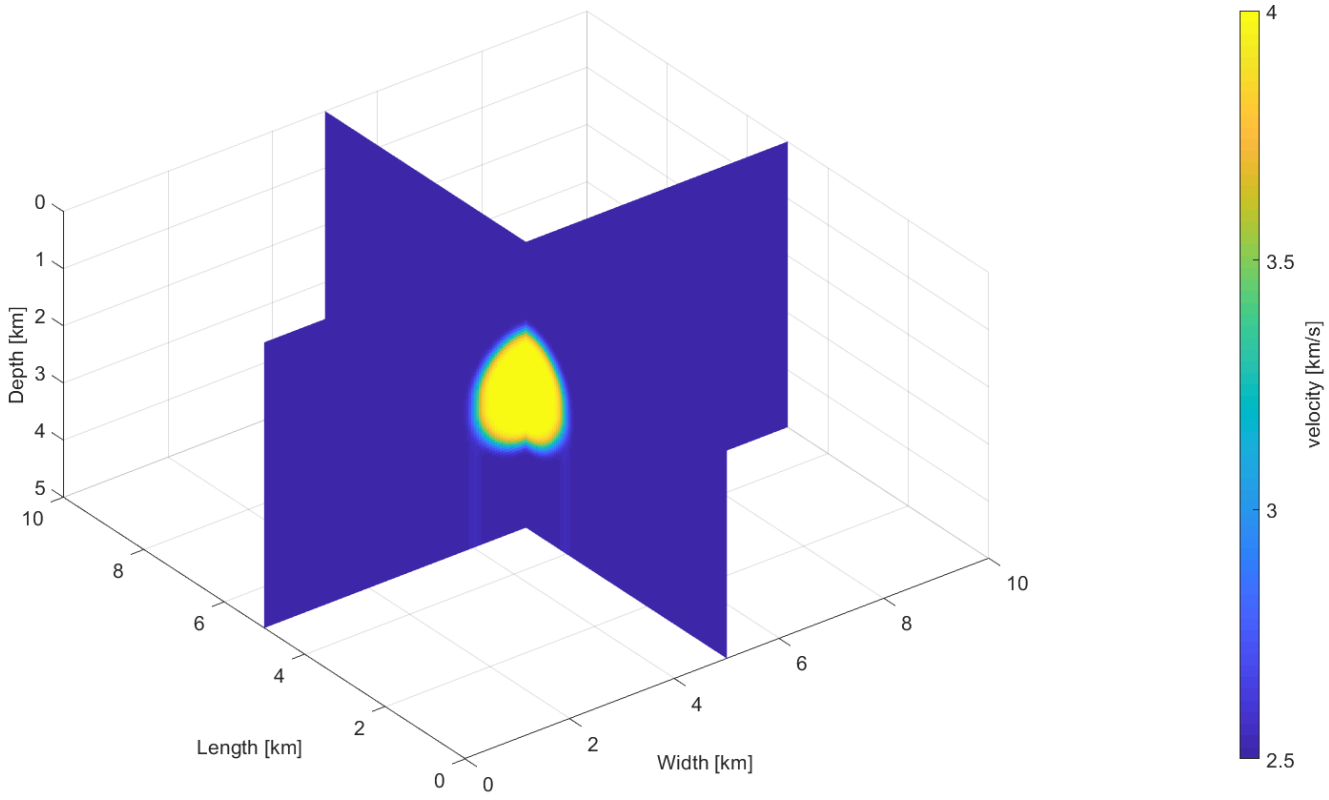

Figure 3.7: *The salt model smoothed with a Hamming radius of 0.3 km.*

4 Results

Conventionally, the cubic spline has been the primary mathematical remedy to represent models for ray tracing. In this chapter, I present results from employing both the cubic and the quintic spline representation in smoothing of velocity models and when accessing the velocity model during ray tracing. I compare smoothing abilities, between the cubic and quintic representation, and present the resulting differences in computed attributes.

4.1 Smoothing ability

To best illustrate the differences between a cubic and a quintic spline function, I employ a smoothing method. This method uses B-splines to represent each grid point in a velocity model. As illustrated in section 3.4, the number of grid points required by the spline depends on the order of the spline. The order of a 1D spline is the degree of the spline + 1 (i.e., the number of elementary pieces the function consist of). The 1D cubic spline requires 4 grid points to represent a model quantity (e.g. velocity) on a grid point interval, whereas the quintic spline needs 6 points.

As a part of the thesis work, I have built the codes to work for both 2D and 3D models. Since the number of calculations are higher for the quintic spline, the computation time will be longer. The number of grid points used for each representation, and the fact that the higher degree spline is stiffer will also yield a difference in the represented value.

The velocity model used in this section, Figure 4.1, to test the smoothing ability, was made in Matlab. It was made with sharp edges to better illustrate the effect of the smoothing ability of the cubic and the quintic spline methods.

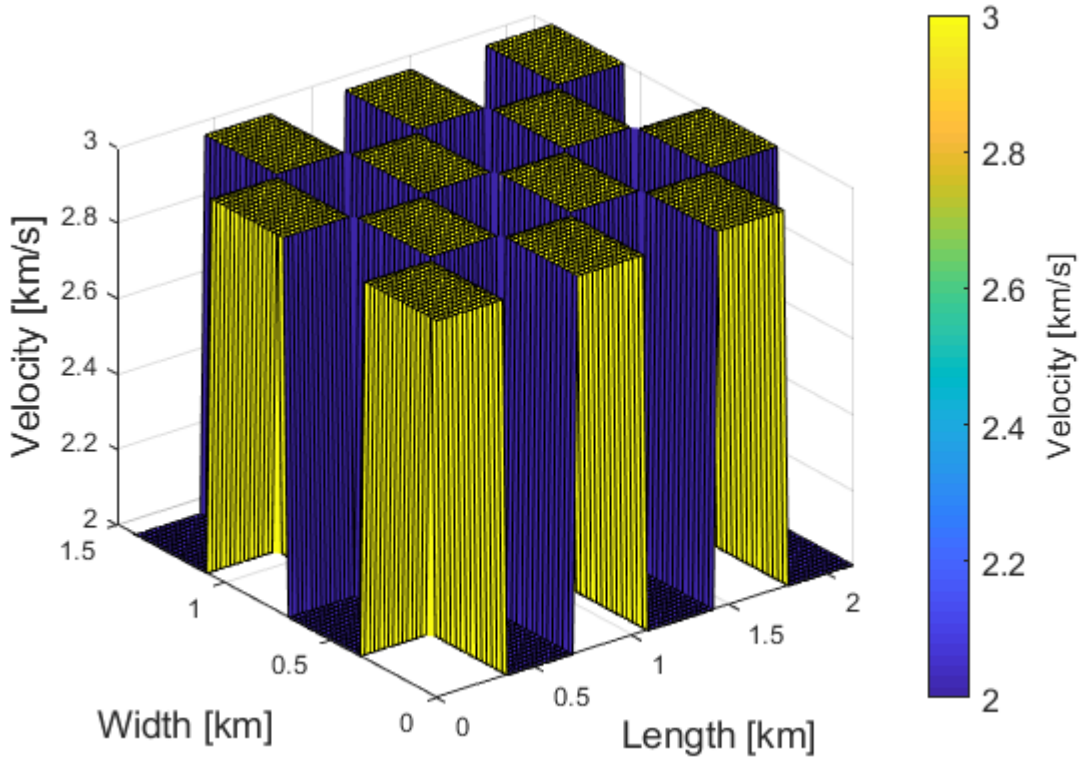

Figure 4.1: *The initial model for testing smoothing ability (Model 0). The model has a width of 1.416 km, length of 2.136 km. The grid spacing in both directions is 0.024 km, and the velocities range from 2 km/s to 3 km/s.*

To get an idea of efficiency and computation time for the two spline representation methods, the models were smoothed through several iterations. The smoothed models illustrated here, see Figures 4.2-4.5, are the result of 1,10,20 and 50 iterations.

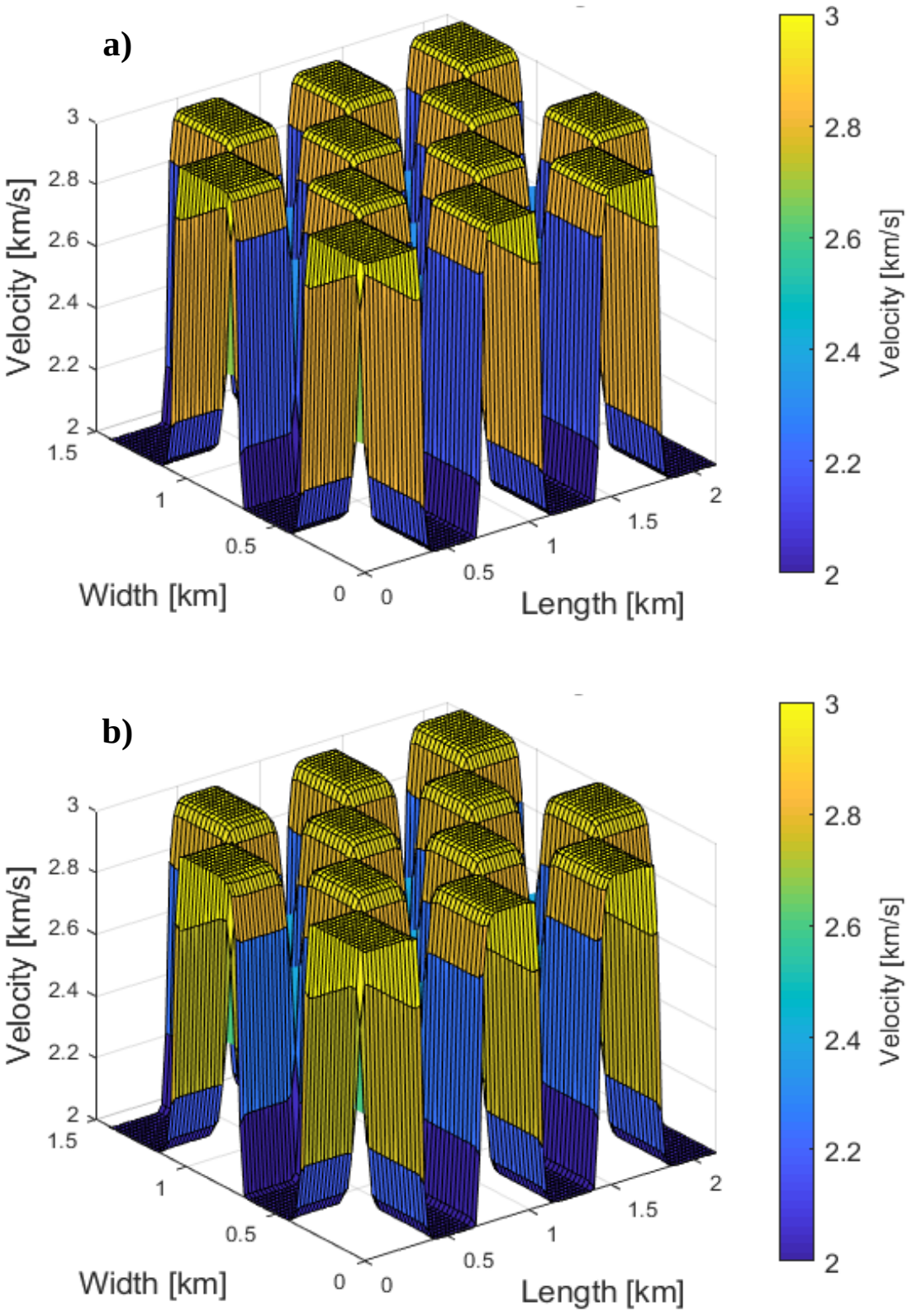

Figure 4.2: *Velocity models after one iteration of smoothing using a) cubic spline and b) quintic spline.*

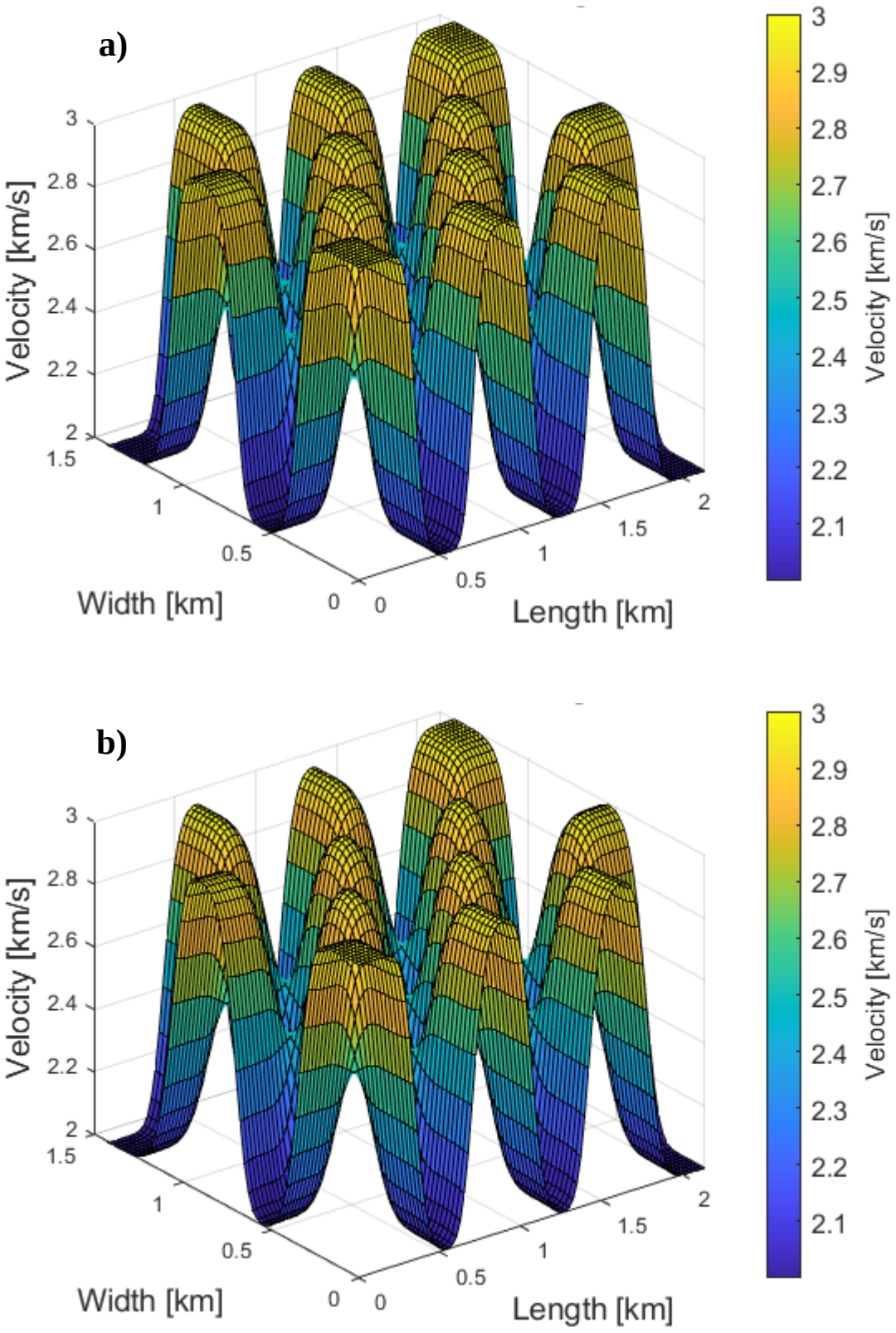

Figure 4.3: *Velocity models after 10 iterations of smoothing using a) cubic spline and b) quintic spline.*

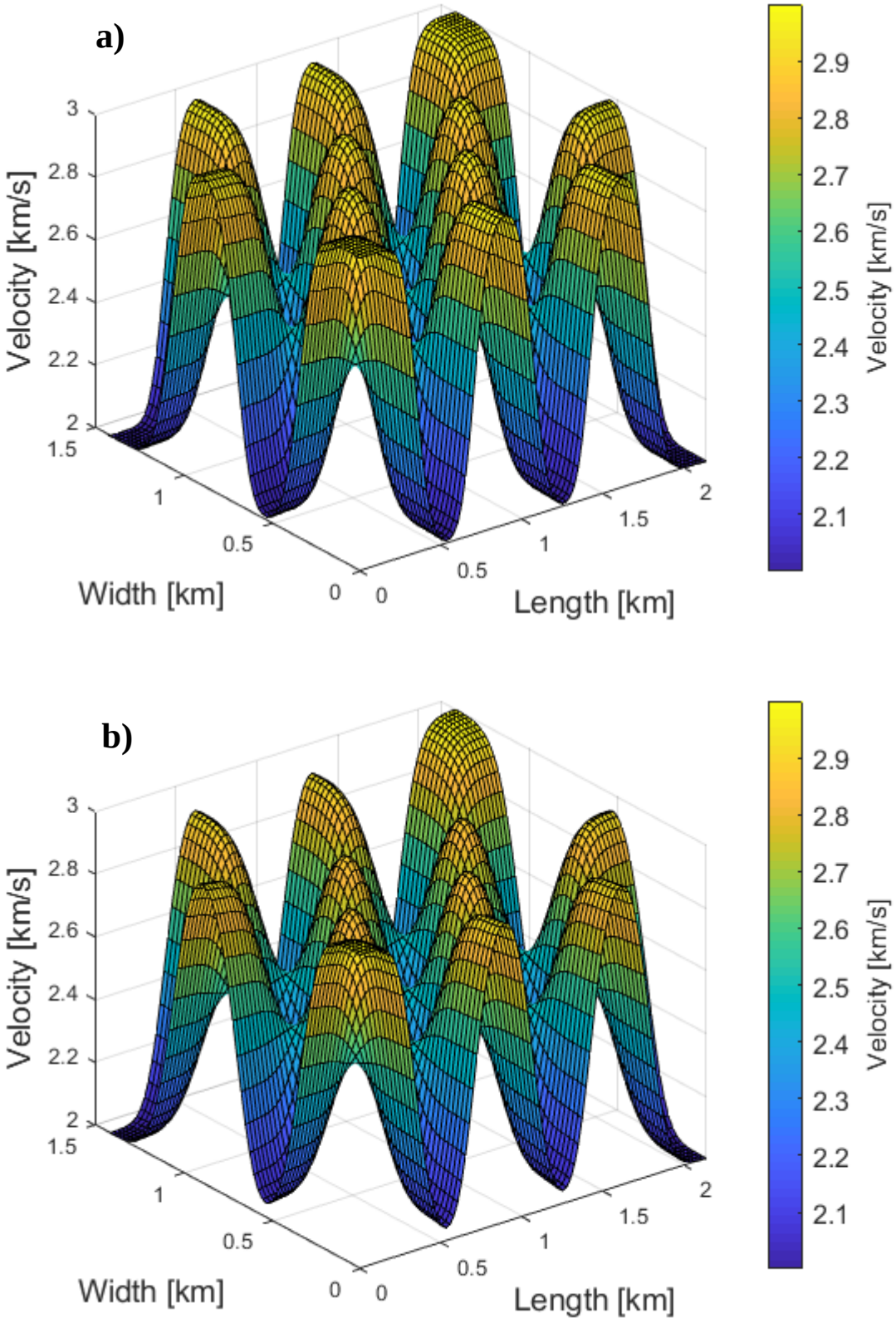

Figure 4.4: *Velocity models after 20 iterations of smoothing using a) cubic spline and b) quintic spline.*

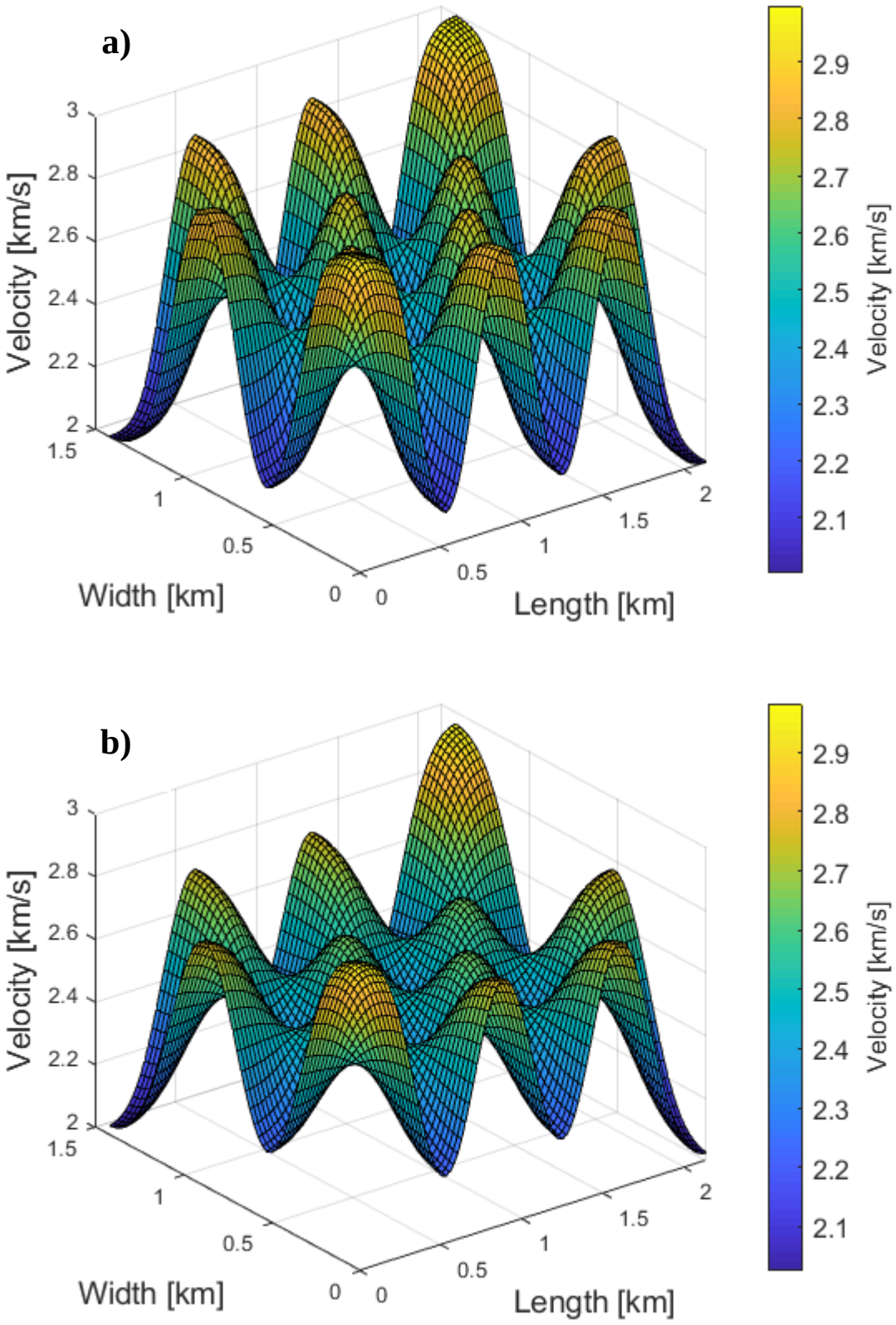

Figure 4.5: *Velocity models after 50 iterations of smoothing using a) cubic spline and b) quintic spline.*

Already from these figures it is apparent that quintic splines representation requires fewer iterations to reach the same degree of smoothness as the cubic spline representation. As mentioned earlier in this section, higher degree splines require a higher number of control points to represent a value, which means that more control points provide contributions to the final representation. This fact paired with the greater stiffness governs the efficacy of the higher degree smoothing method. This is due to the fact that the integral of the B-spline basis function always is one, and the quintic spline requires a larger interval so that the highest absolute value of the basis curve is always smaller than for a cubic spline.

For measuring the smoothing ability, we used the relative variance. The variance measures the square of the distance, for a random variable *X*, from its mean (Adams and Essex, 2013). The variance can be written as

$$\sigma^2 = \sum_{i=1} (X_i - \mu)^2 f(x)$$

where μ denotes the mean of *X*, *f(x)* is the probability function and σ^2 is the variance. The variance measured below is calculated relative to the variance of the initial model, model 0. We can write that the relative variance equals ${\sigma^2}_{model\ (n)}/{\sigma^2}_{model\ (0)}$.

The difference in smoothing ability is presented graphically in the figure below.

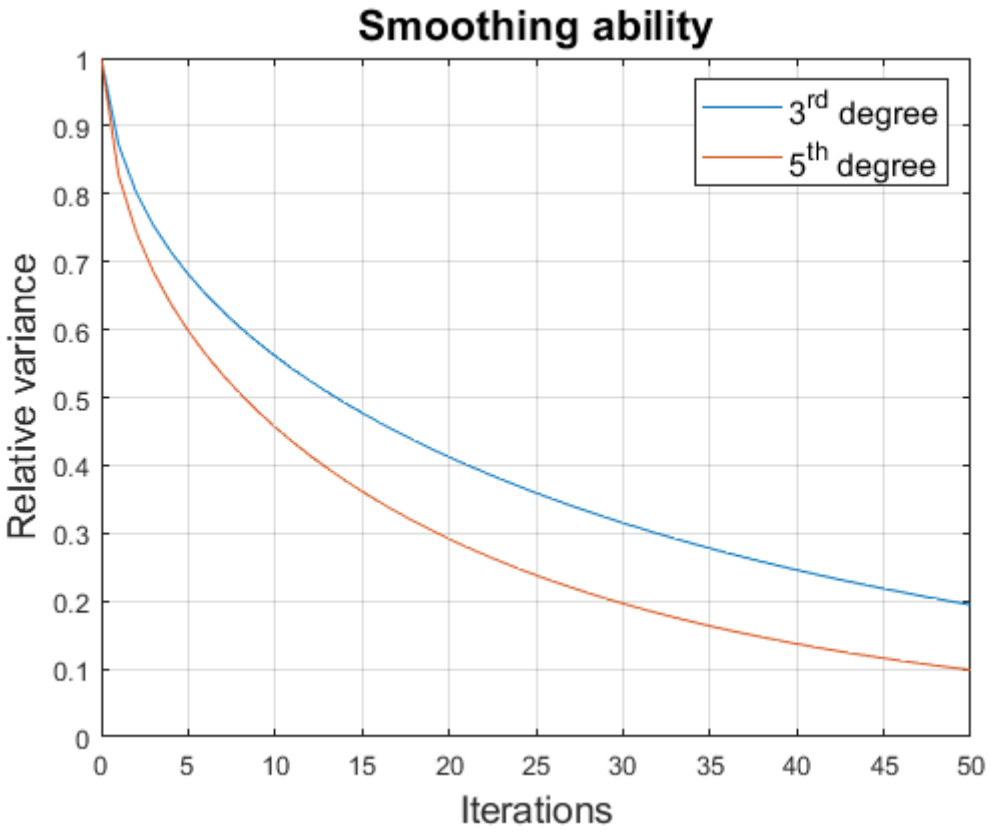

Figure 4.6: *Graph displaying the relative variance from the mean of the initial model as a function of iterations for the cubic and the quintic spline representation method.*

Figure 4.6 illustrates how many iterations the two spline representation methods require to reach the same level of smoothness (i.e. how many iterations to reach the same relative variance from the mean of model 0).

The figure shows that the lower degree method requires more iterations to obtain the same level of smoothness as the higher degree method. Even though the quintic spline method required fewer iterations for the same degree of smoothing, it was not faster.

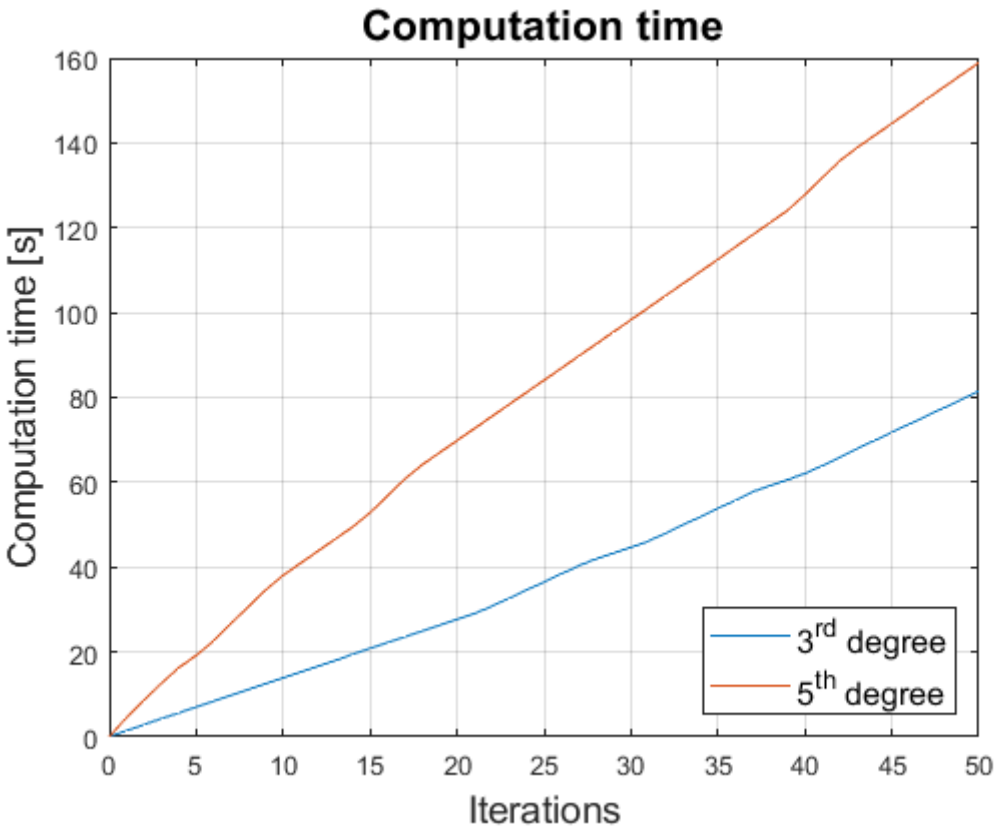

Figure 4.7: *Graph displaying computation time as a function of iterations for the cubic and the quintic spline representation method.*

In Figure 4.7, above, the computation time for the two smoothing methods is presented as a function of iterations. It is clear that the higher order method requires a lot more computation time. In the figure below I set the relative variance to a fixed value. This resulted in two models of the same level of smoothness, and is a good representation of how the computation time differs between the two methods.

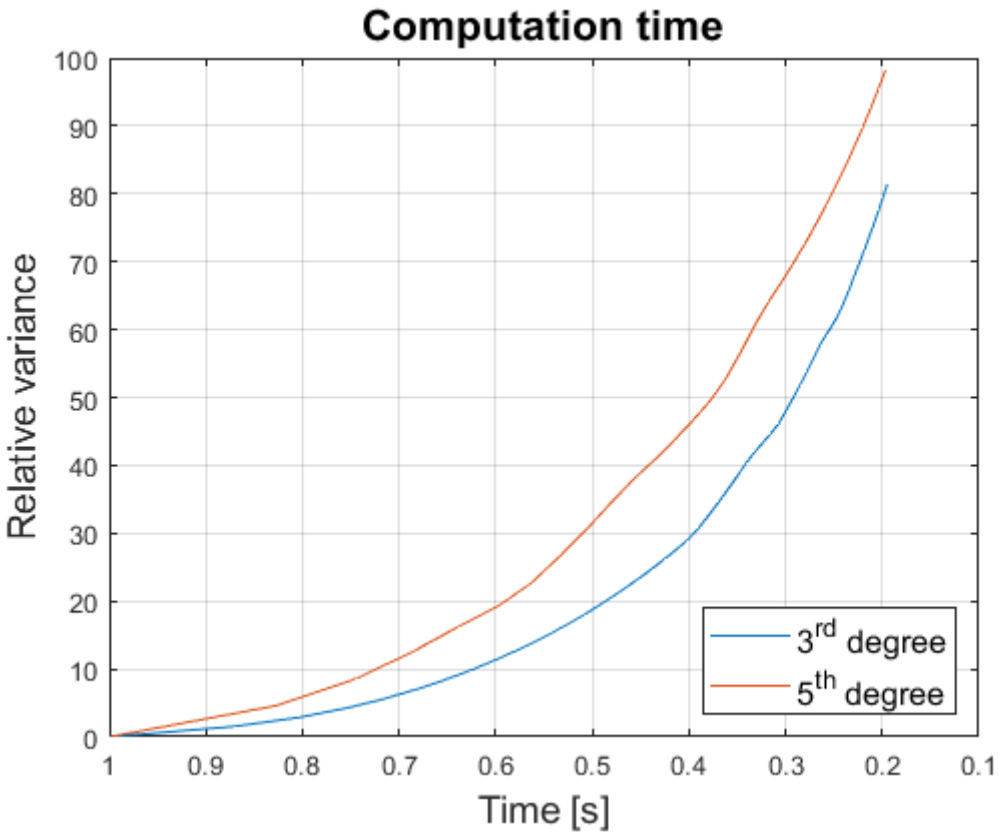

Figure 4.8: *Graph displaying the computation time relative to the smoothness (relative variance) for the cubic and the quintic spline representation methods.*

From the Figure 4.8 we see that the quintic spline representation requires more computation time than the cubic to reach the same level of smoothness.

4.2 Two-point Ray tracing

To properly test the effect the use of higher order spline representation has on seismic attributes, I have built a Matlab function for two-point ray tracing. Initially the modelling was done in NORSAR-3D in order to compare and validate the Matlab ray tracer. This was a crucial step prior to implementing the quintic splines.

From NORSAR-3D I extracted source position, initial slowness, slowness at receivers, receiver position and travel time. The models used in this thesis, presented in section 3.5, were also smoothed in NORSAR-3D to be suitable for ray tracing. The goal of the Matlab ray tracer was to produce as similar a result to the extracted data as possible, using the same model, and the same initial values.

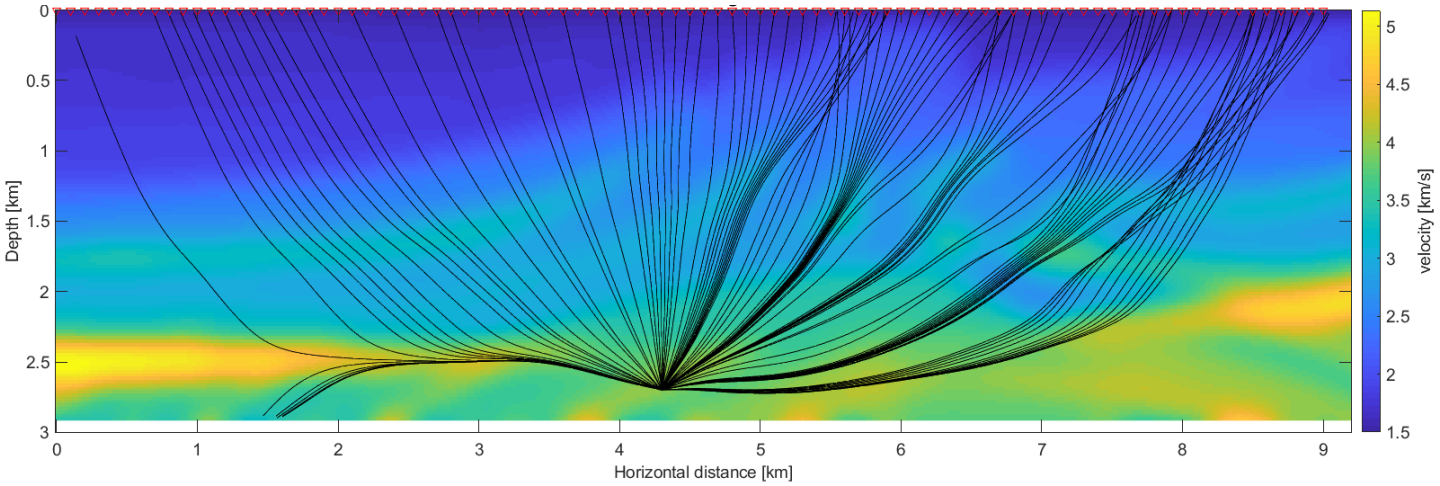

Figure 4.9: *Rays from direct ray tracing in the Marmousi model using cubic spline representation with initial values extracted from NORSAR-3D.*

The ray tracer in Matlab was tested with the same initial slowness and travel time as in NORSAR-3D. Figure 4.9 illustrates resulting rays of the ray tracing in the Marmousi model. As can be seen in the lower left corner of the figure, not all the rays reached the surface. The high velocity zone proved a challenge for the Matlab tracer.

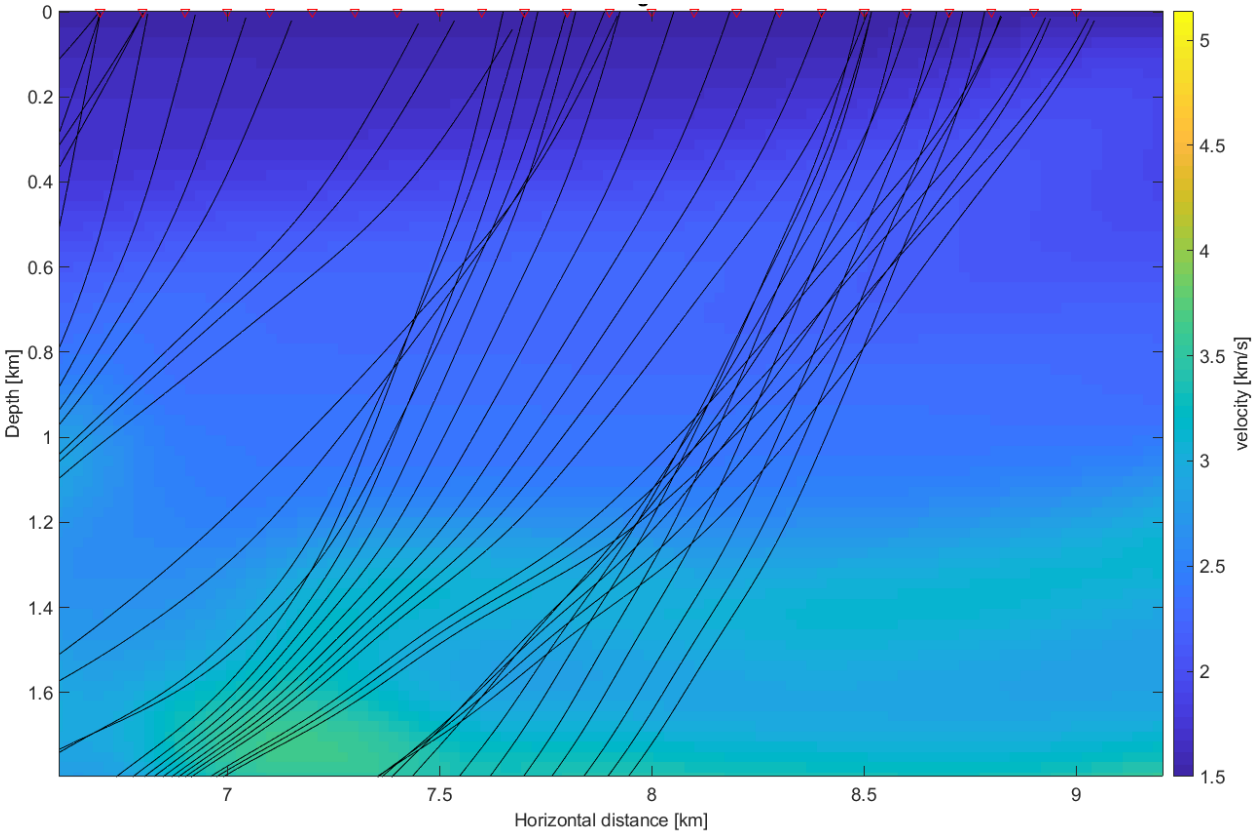

Figure 4.10: *Zoom in of the upper right corner of Figure 4.9, displaying the deviation between ray end points and receivers.*

As can be seen in Figure 4.10, the rays that reached the surface did not deviate far from the receivers. The rays where compared to and found to be close to the data extracted from NORSAR-3D. For a realistic simulation, it is desirable for the rays to reach a receiver with a deviation as small as possible.

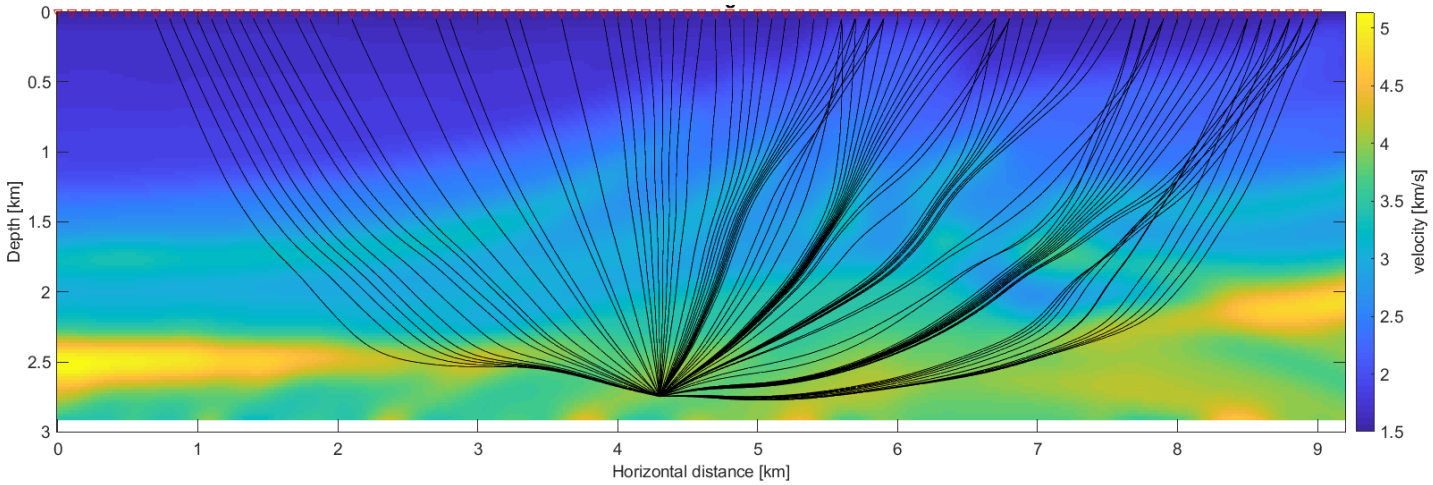

Figure 4.11: *Rays from two-point ray tracing in Marmousi model, using cubic spline representation and initial values extracted from NORSAR-3D.*

In the two-point ray tracer I sat the deviation tolerance to 5 m. (the straight line from the end point of the ray, to the associated receiver). After implementing this ray tracer, the NORSAR-3D results and the Matlab result were sufficiently similar. The travel time and slowness at the receivers were both acceptably close to the extracted NORSAR-3D values. The last quality check of the tracer was to trace rays backwards from their endpoint. If the calculations for the dynamic ray tracing are done correctly, the relative geometrical spreading from source to receiver should be equal to the relative geometrical spreading from receiver to source. Testing this proved conclusive, the geometrical spreading was equal in reverse.

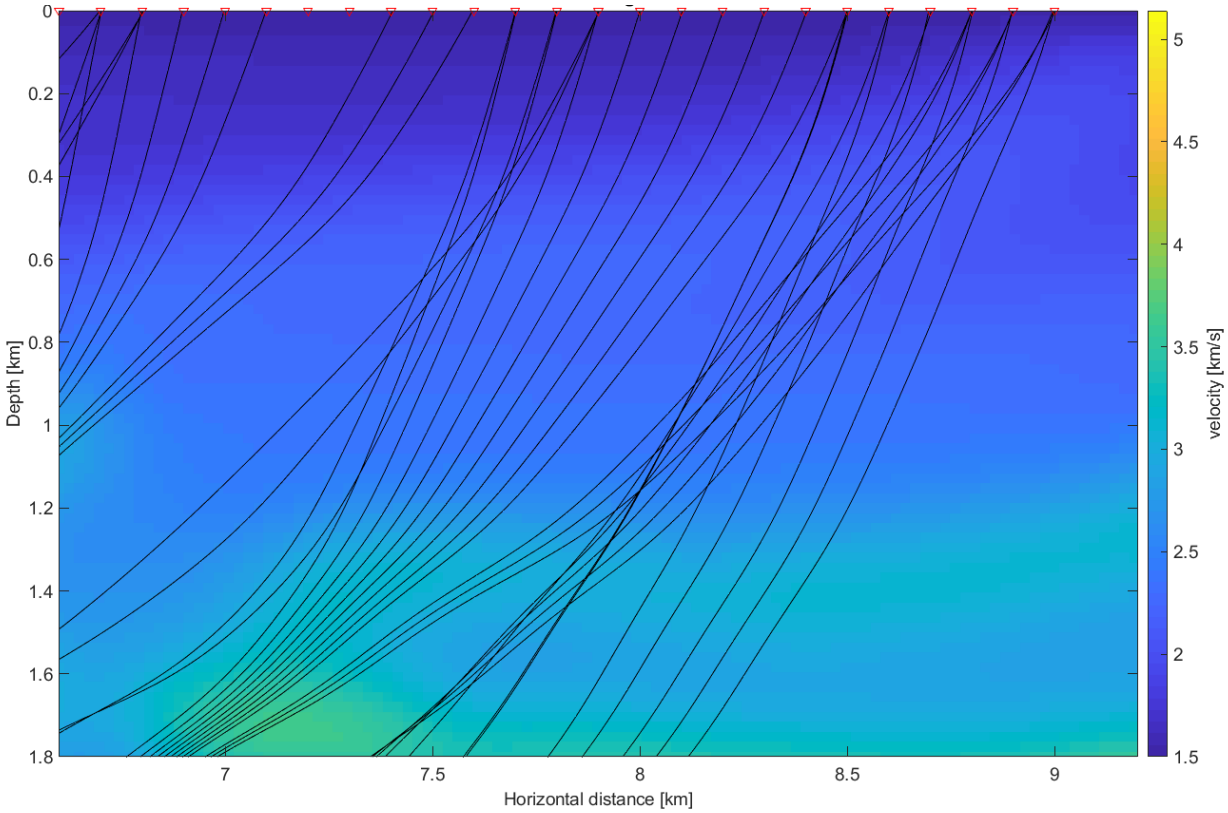

Figure 4.12: *Zoom in of the upper right corner of Figure 4.11, displaying the rays and receivers after two point ray tracing.*

4.2.1. Test of robustness

To accentuate the differences in robustness between the quintic and the cubic spline representation, an anomaly is introduced to the velocity model. To properly compare the two representations, the rays in the initial model have the same source position and the same receiver position. The test starts with 200 rays for both the cubic and the quintic representation. For each time the anomaly changes, the rays have the same initial slowness and is bound by the same receiver. The iterations required for each ray to reach their respective receiver is summed together, and number of rays reaching their receiver are counted for each new anomaly. The findings of this test are presented in the following table.

	Cubic spline representation		Quintic spline representation	
Size Anomali [km/s]	**Sum Iterations**	**Rays reaching receivers**	**Sum Iterations**	**Rays reaching receivers**
-2	498	196	375	200
-1,5	418	198	309	200
-1	369	199	272	200
-0,5	265	200	223	200
0	200	200	200	200
0,5	273	200	223	200
1	327	197	281	200
1,5	402	198	299	198
2	410	196	333	198

Table 1: *The table show the number of rays reaching their receiver, and the sum of the iterations the rays needed for the different magnitude of the anomaly.*

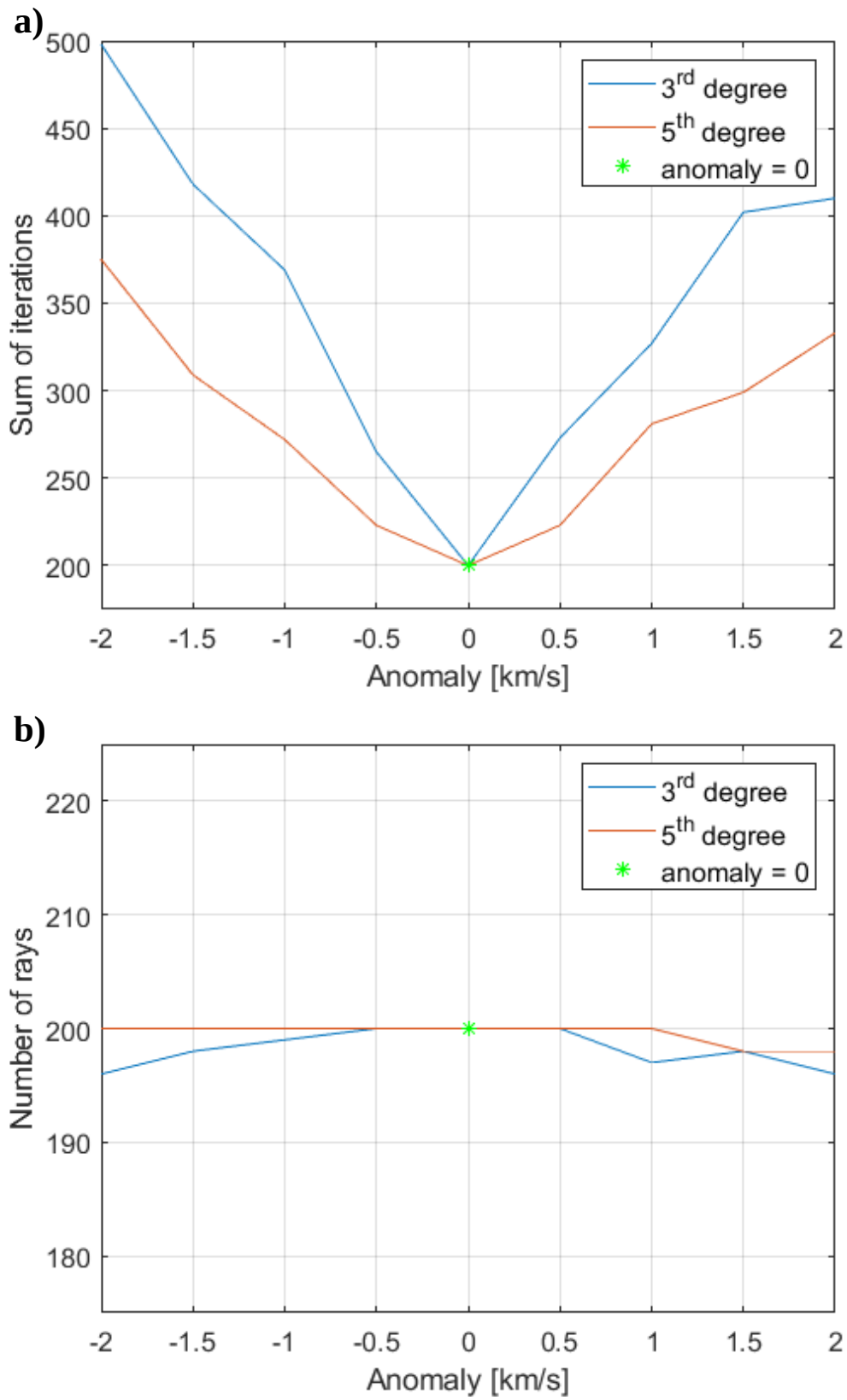

Figure 4.13: *Graphical display of a) the total number of iterations as a function of the size of the anomaly and b) the number of rays that reach their receiver as a function of the anomaly, for the cubic (blue) and the quintic (red) representation.*

The results presented in Figure 4.13 are a graphical display of Table 1. The graphs show that the quintic spline representation are more stable considering strong local variations in the velocity field. The amount of iterations needed when the magnitude of the anomaly increases, are fewer for the quintic representation compared to the cubic representation. To ensure that the two-point ray tracing did not diverge, the limit for the number of iterations per ray was set to five. This means that the rays that did not reach a receiver was counted as five in the sum of iterations. The number of rays that reach a receiver is also more stable for the higher degree representation. For the eight tests, the rays using quintic representation managed to find all their receivers in six of the tests, while the rays using cubic representation only managed this in two tests.

4.3 Ray path and velocity

From the previous section, the greater stability of the quintic spline representation was presented. An important part of this study is to also test the effect the quintic spline have on the seismic attributes. As the cubic spline is the traditional representation method in ray tracing and a trusted method, the attributes calculated using quintic representation should not deviate to far from the attributes found using cubic representation.

4.3.1 Marmousi model

The differences in attribute values caused by the different continuity properties in the models were found to be quite small in the softest of the two Marmousi models. This could be because of the density of grid points, as the grid spacing is quite small in Marmousi. In this sub-section, I will present the results from the softest of the Marmousi models, as well as a manipulated (perturbed) model. In the perturbed model, the grid spacing in the horizontal direction is 96 m (every fourth grid point) and in the vertical direction the grid spacing is 72 m (every third grid point).

To compare the two methods, it is important to use the same rays. This is done by numbering the rays found using cubic spline representation. For the quintic representation, the exact same initial values and receivers are used, and the ray-number of the rays reaching their receivers are saved as an array. Before the comparisons are done, the rays are sorted so that the ray

number arrays match for the cubic and quintic representation. The following figures present the difference in ray path and the difference in velocity representation along the rays.

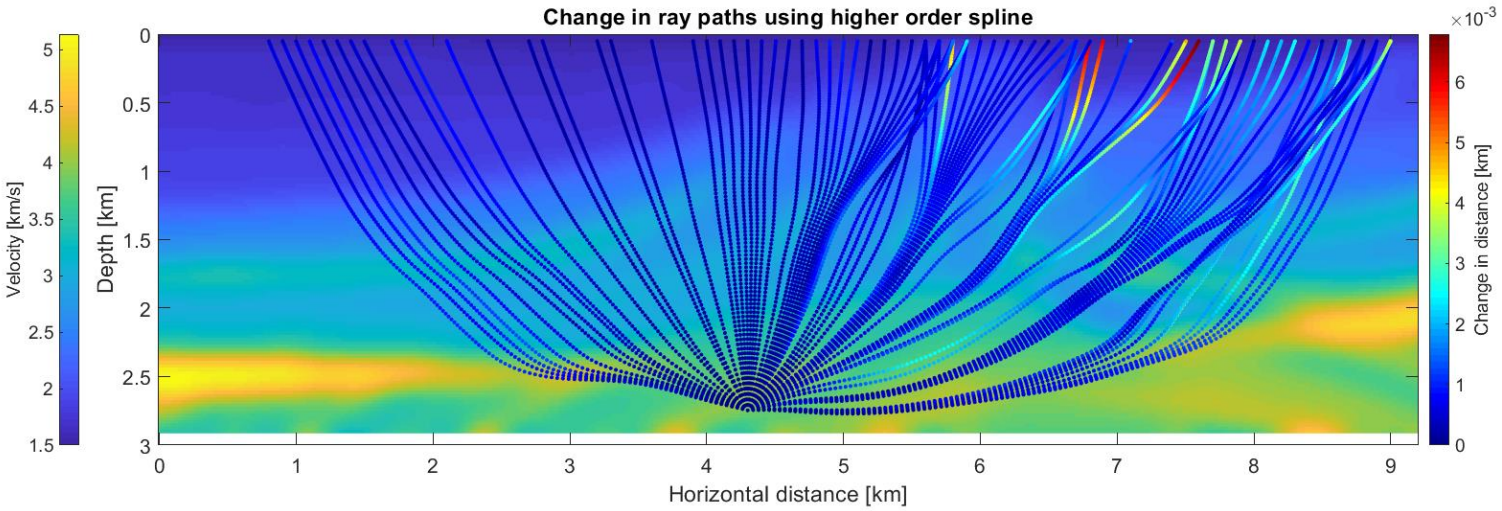

Figure 4.14: *Deviation in ray path using quintic spline representation relative to cubic spline representation in the soft Marmousi model.*

The figure above, Figure 4.14, illustrates the change in distance for the ray paths using quintic instead of cubic spline representation. The colorbar on the right side reveals that the difference in raypath is quite small, with a deviation of approximately six meter at most.

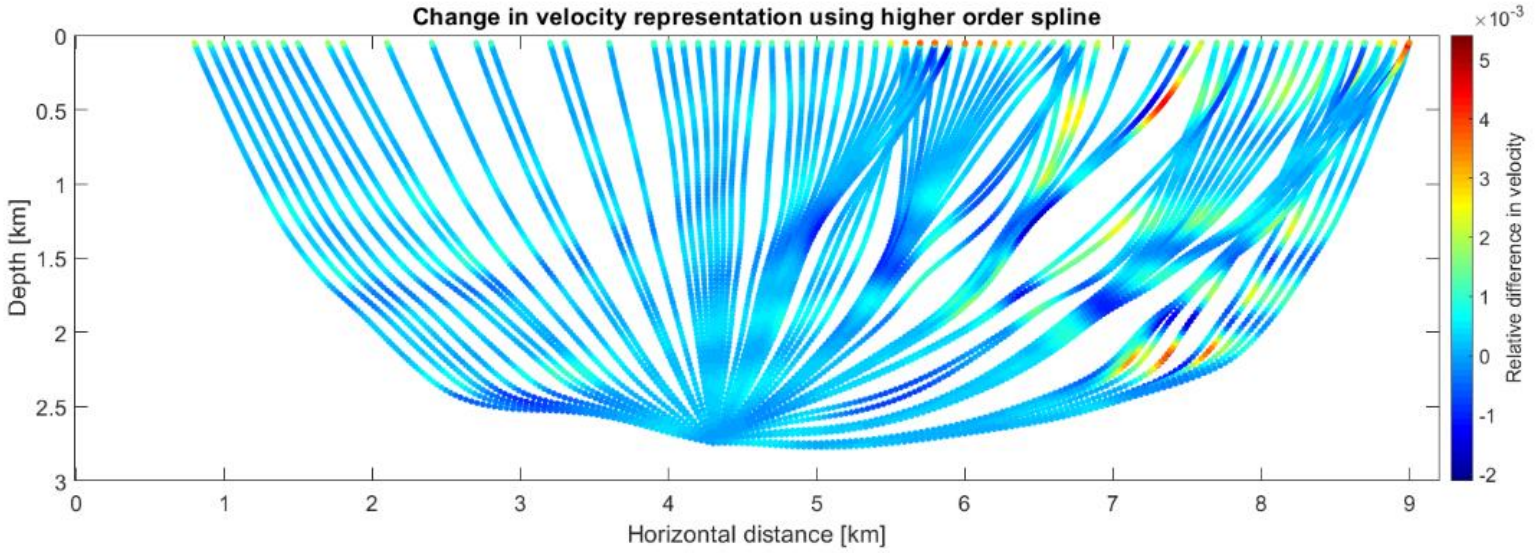

Figure 4.15: *Difference in velocity representation using quintic relative to cubic spline representation in the soft Marmousi model.*

Figure 4.15 illustrates where the velocity representations along the ray paths differs for the higher degree splines. The differences in velocity correspond to the differences in ray path. In the Marmousi model there are quite large velocity variations over small distances. This means that the differences we see in the model are expected. The higher degree spline representation requires information from more grid points, which means that a larger area of the model is considered when representing a query point.

If we manipulate the Marmousi model, and only consider every third or fourth grid point, the significant and rapid variation in velocity in the Marmousi model become more prominent. As a result of this, the differences between attributes resulting from the cubic and quintic spline representations should be more clearly observable.

A manipulated model was made, where in the vertical direction, only every third grid point was used. In the horizontal direction, every fourth grid point was used and the grid spacing was modified proportionally to maintain the model dimensions. This manipulation made it harder to perform a successful two-point ray tracing, as the larger grid spacing made the model less smooth. A "harder" model leads to more uncertainties when perturbating the incident angle.

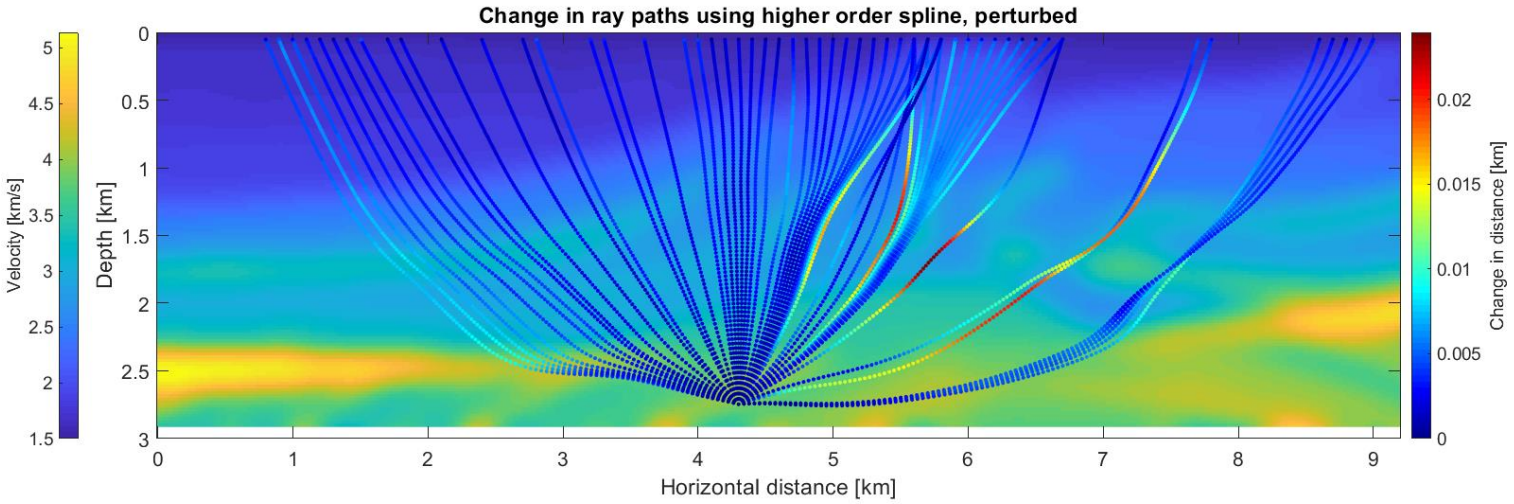

Figure 4.16: *Deviation in ray path using quintic spline representation relative to cubic spline representation in the perturbed Marmousi model.*

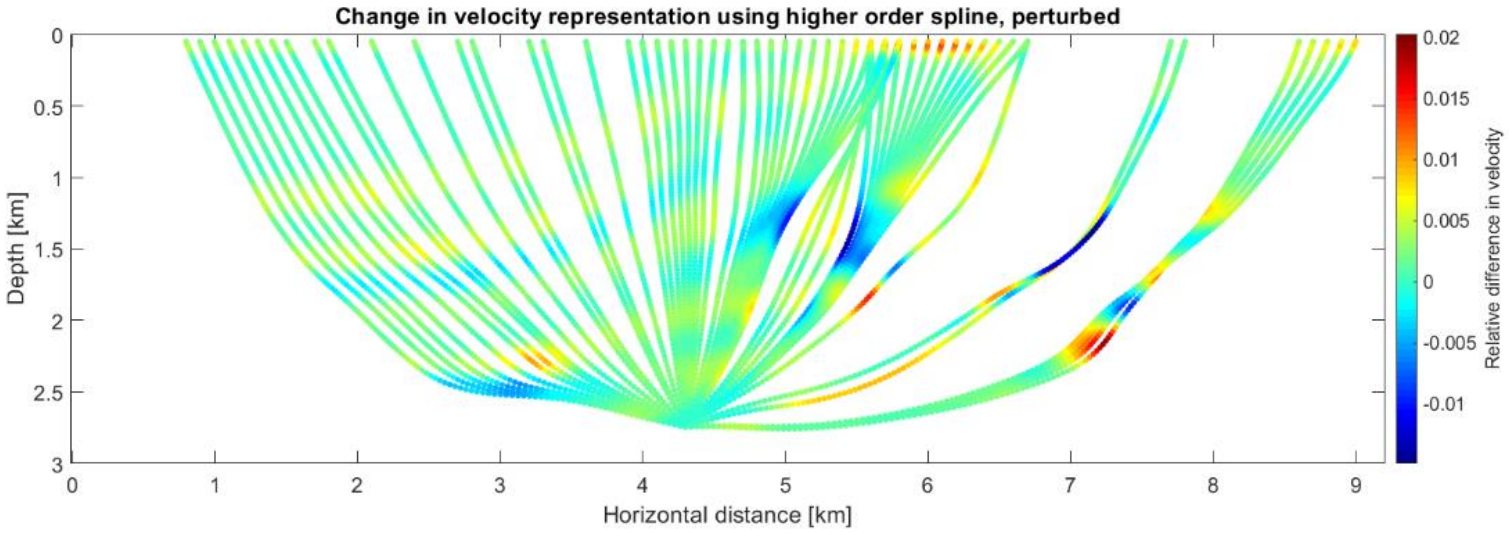

Figure 4.17: *Difference in velocity representation using quintic relative to cubic spline representation in the perturbed Marmousi model.*

The perturbed models in figures 4.16 and 4.17 are presenting similar results as the original models. Though there are fewer rays in the perturbed model, compared to the soft model, the differences occur in the same place, but are more accentuated.

4.3.2 Salt model

In the salt model, the ray tracing was done with a fixed travel time. The travel time was set to 1.5 seconds, the source point was set to x=4.5 km, and z=4.7 km. The deviation between the lower and the higher order spline was, also in this model, quite small. In terms of the ray path, this could have to do with the fact that the velocity is mostly constant away from the salt sphere. As for the Marmousi, a perturbed model was made for the salt model as well.

The perturbed salt model had a grid spacing of 100 metres, which correspond to every second grid point in the original salt model.

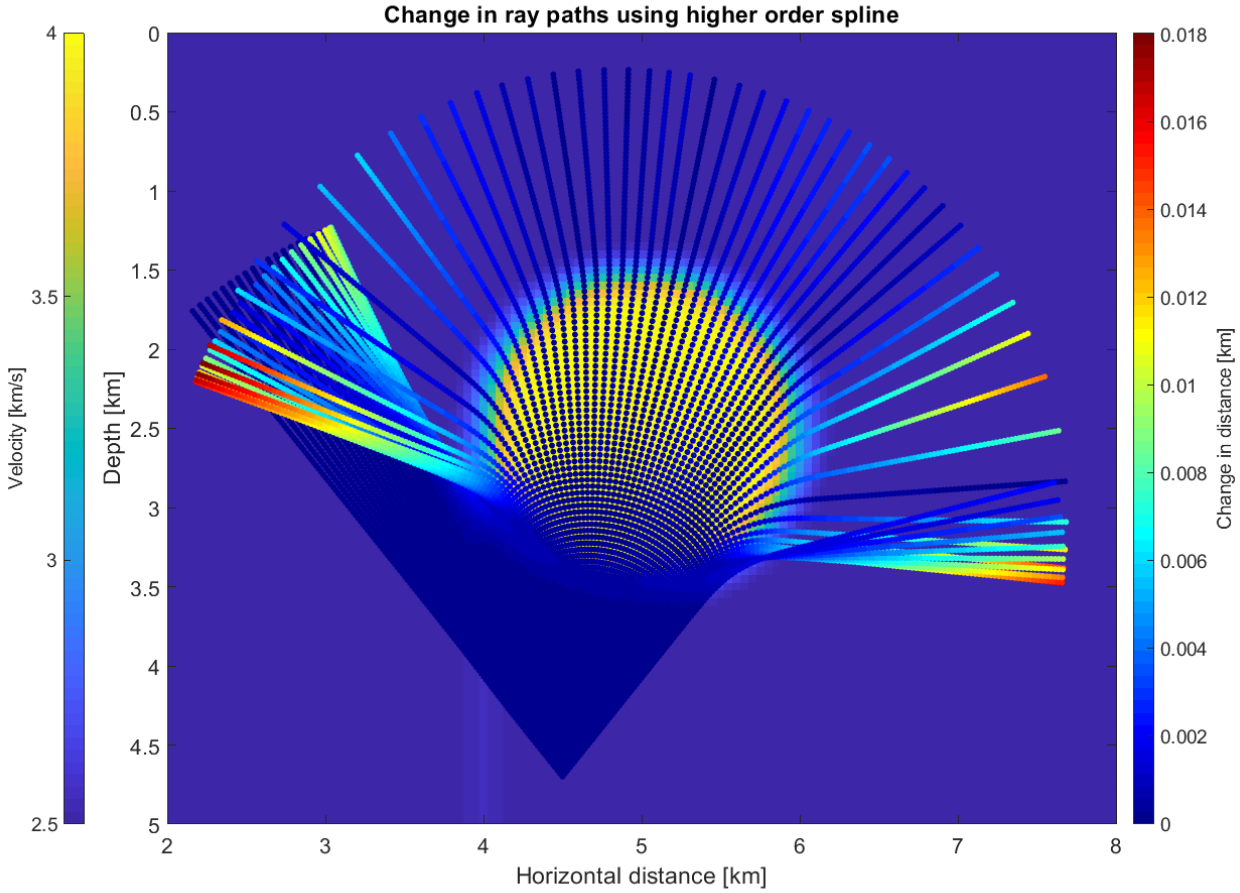

Figure 4.18: *Deviation in ray path using quintic spline representation relative to cubic spline representation in the salt model.*

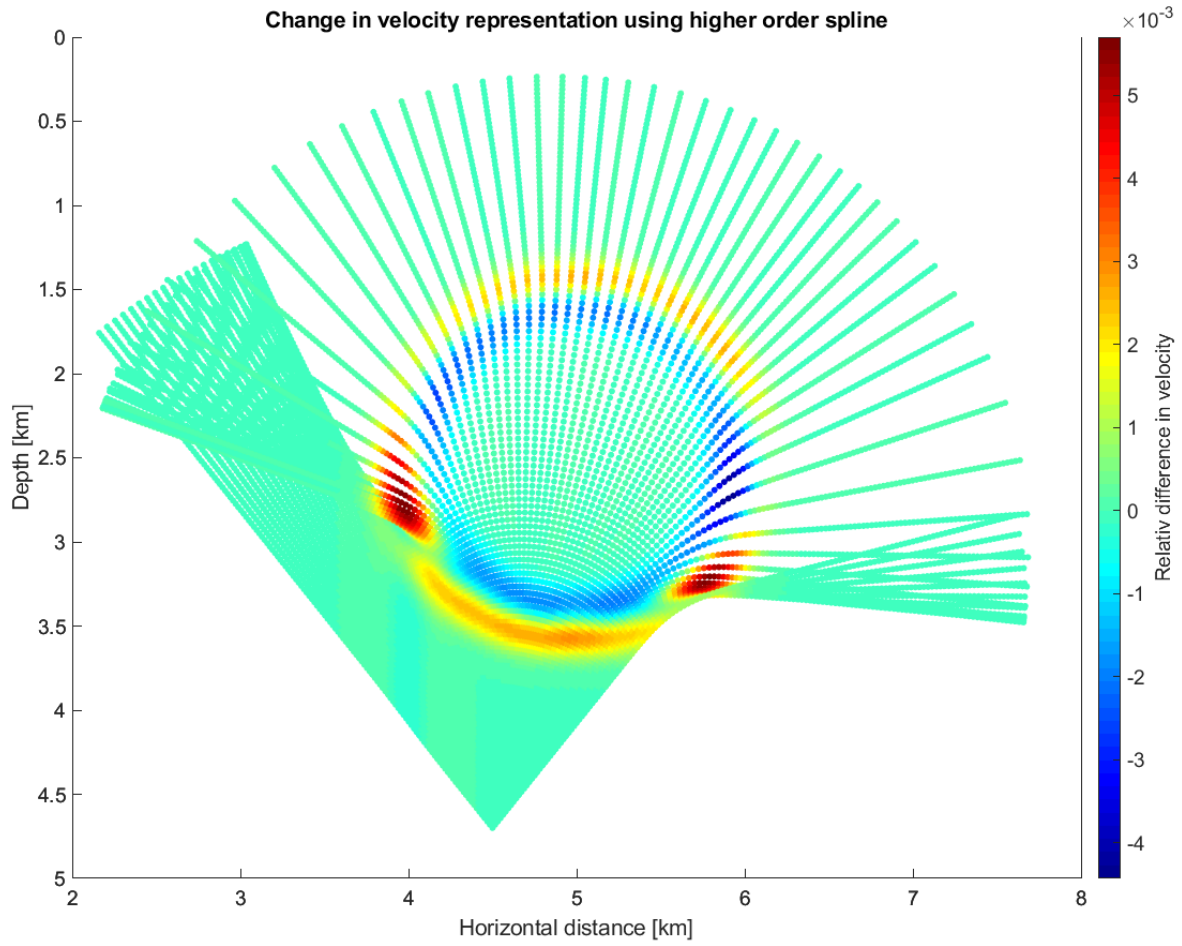

Figure 4.19: *Relative difference in velocity representation using quintic relative to cubic spline representation in the salt model.*

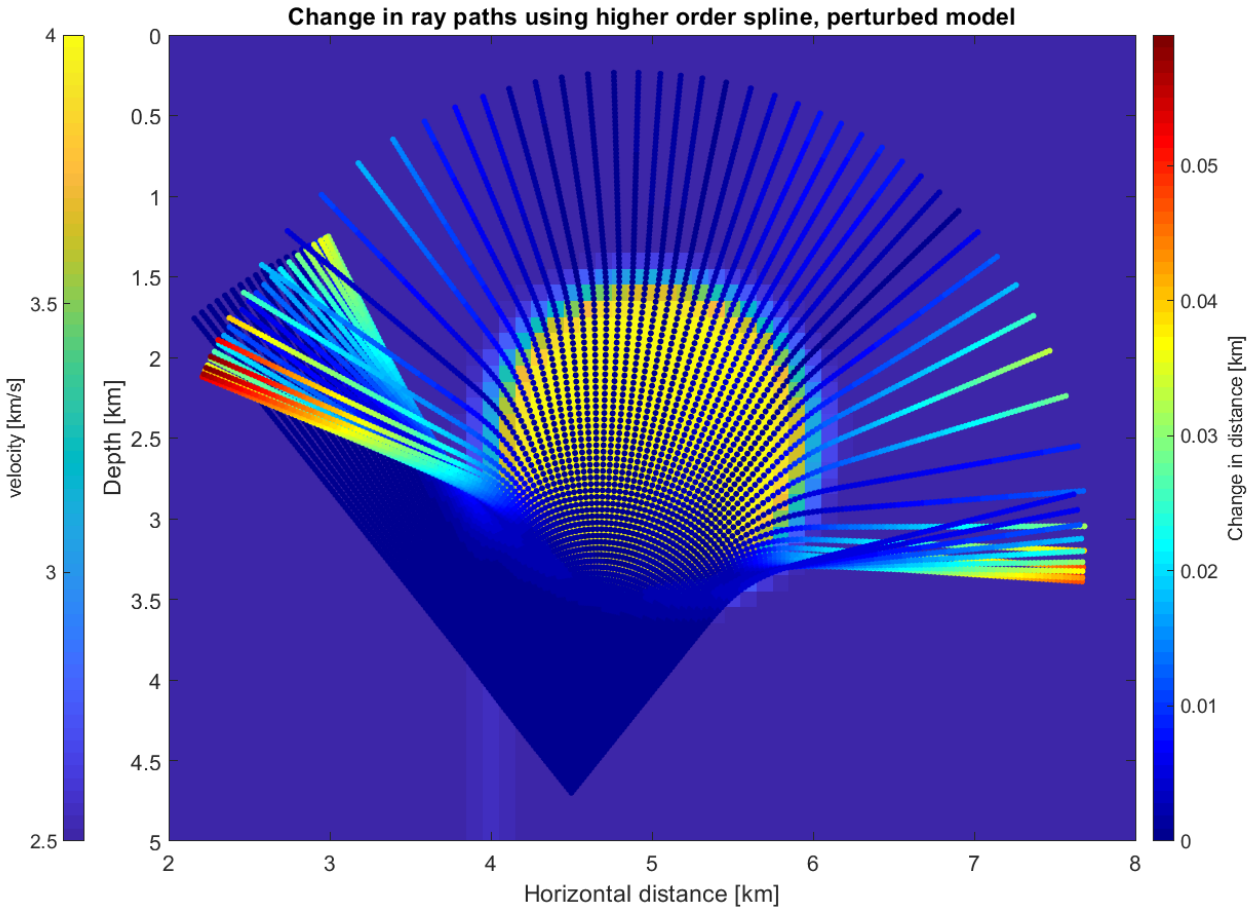

Figure 4.20: *Deviation in ray path using quintic spline representation relative to cubic spline representation in the perturbed salt model.*

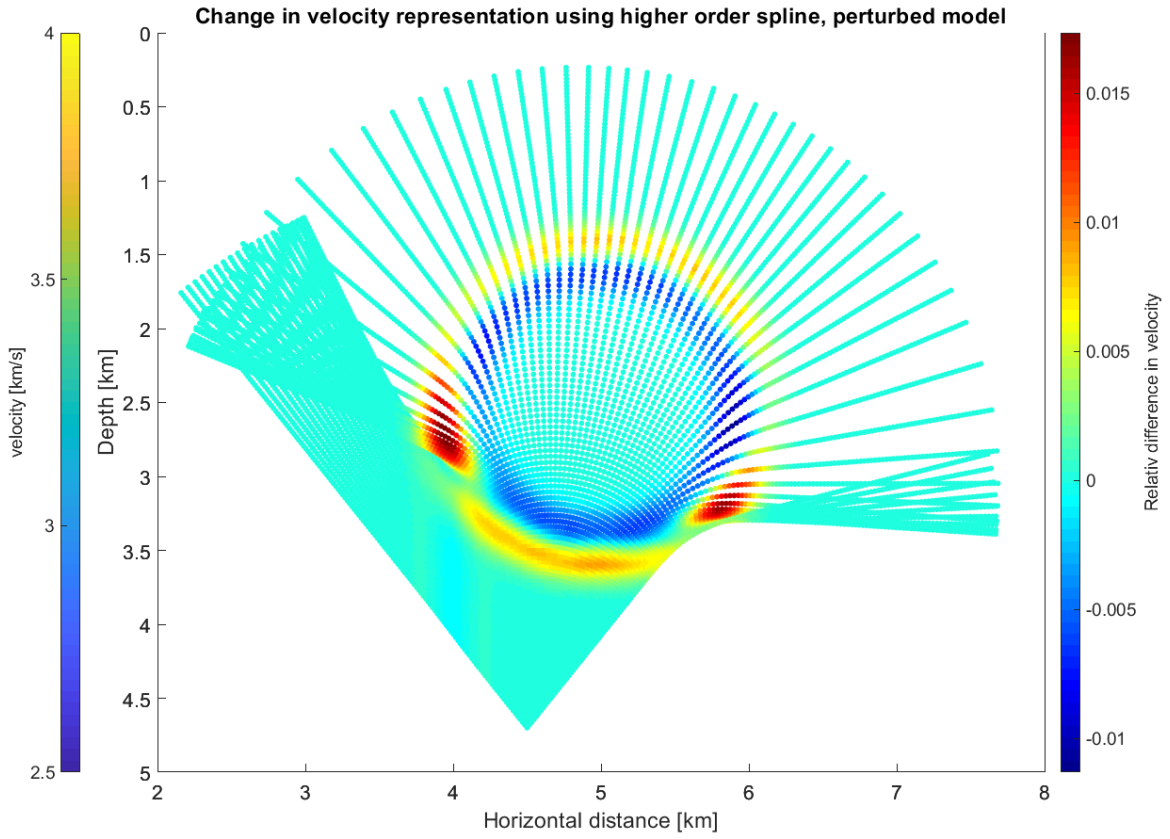

Figure 4.21: *Relative difference in velocity representation using quintic relative to cubic spline representation in the perturbed salt model.*

As can be seen from Figures 4.18-4.21 the results are similar to those in the Marmousi model. The perturbed model emphasizes the differences in velocity and the associated deviations in ray paths.

In Figure 4.19 and 4.21 the differences in the behaviour of the splines near a severe velocity shift is accentuated. In the dark blue areas, the quintic spline represents lower velocities as opposed to the cubic spline, while in the orange/red areas the quintic spline represents higher velocities. Though the differences in ray path and velocity are small, they could have a larger effect on attributes like amplitude, where even small variation can result in a large consequence.

4.4 Amplitude

The differences illustrated in the velocity plots in the previous section suggests that the amplitude calculations should be affected as well. The amplitude depends on the velocity and geometrical spreading, see section 3.3. The models used in this thesis is assumed to have a constant density. To best present the differences in amplitude, the salt model is used. The simplicity of the model makes it easier to interpret how the amplitudes are affected using the higher degree representation. Again, to accentuate the differences, the perturbed salt model is used.

Figure 4.22 illustrates the difference in amplitude with respect to ray path (b), and as a function of slowness in the source and travel time (a). In the salt model, the wavefront is "folded" due to the curved velocity contrast of the salt sphere. This shift makes the wavefront concave in the fold. Where the rays crosses in this way with the determinant of **Q** equal zero, are called a caustic (Červený, 2001). Equations 3.24 and 3.25 shows that when the determinant of **Q** approaches zero, $\mathcal{L}(R,S)$ approaches zero, and amplitude approaches infinity.

In the Matlab tracer I sat a lower limit to the geometrical spreading to avoid it to be zero. The amplitudes of the ray peak around the fold of the wavefield. As can be seen in Figure 4.22, below, the relative difference in amplitude between the cubic and the quintic spline representation is quite big around the fold in the wavefield.

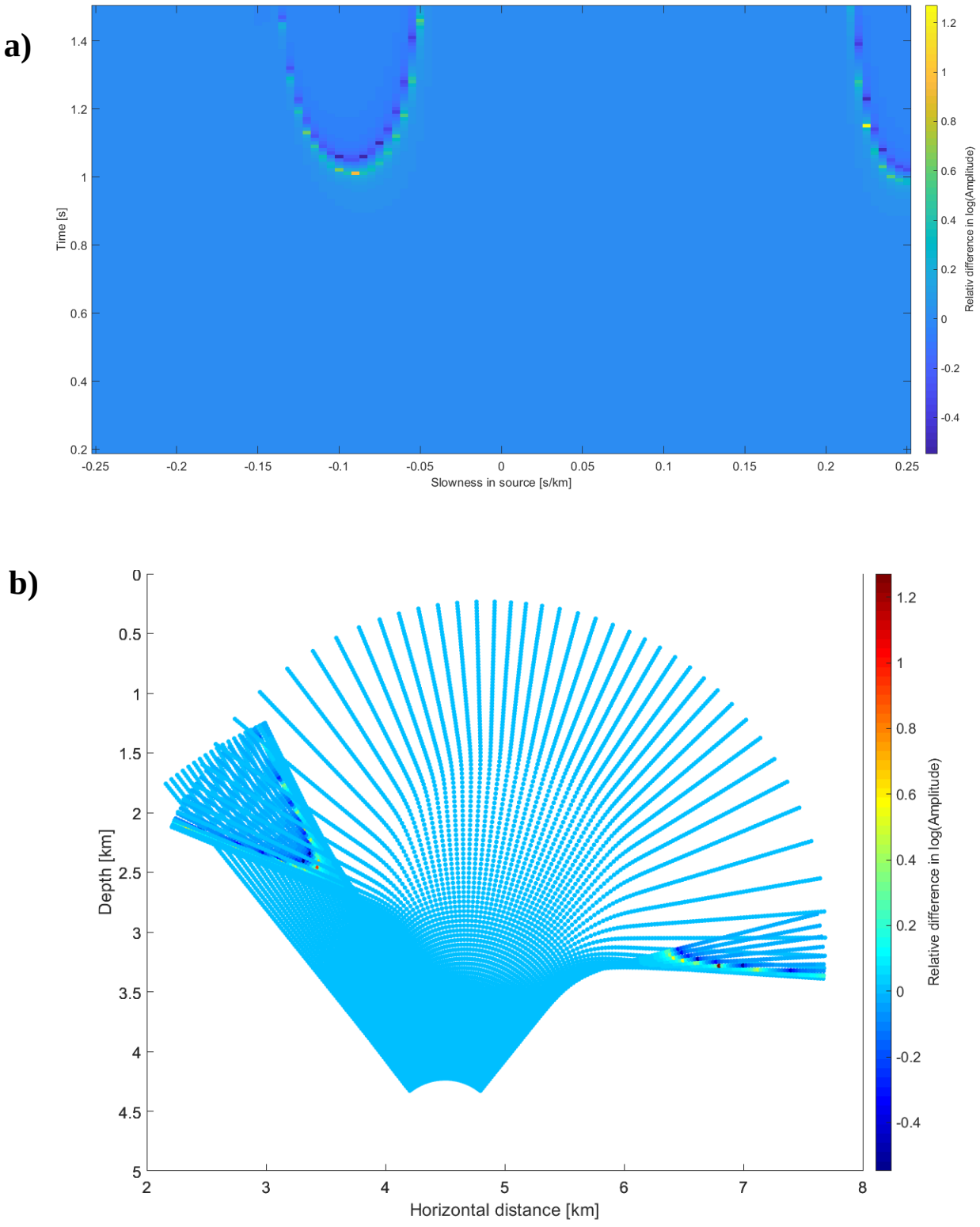

Figure 4.22: *Relative difference in amplitudes a) as a function of travel time and slowness and, b)as a function of ray path, using cubic and quintic spline representation.*

4.4.1 Seismograms

To further study the differences in amplitudes, two-point ray tracing was done in the perturbed salt model. The receiver spacing was set to 25 m. and resulted in 95 traces. The seismograms were made using the package SeisLab in Matlab. To properly compare the results for the cubic and the quintic representation it is important that the exact same rays are used. This was done in the same way as in section 4.3, where each ray for the cubic representation has its own number, and the same initial conditions and boundary conditions are used for the quintic representation. For the seismogram, information about caustics was needed for the proper phase of the amplitude. The Matlab codes for computation of traces and the codes for identification of caustics were provided by Einar Iversen, as an implementation of the equations from section 3.3 equations (3.30-3.32). For the source pulse, a 25Hz Ricker wavelet, implying a wavelength of 100 m was used. Because the magnitude of the amplitude varied enormously due to caustics, the high amplitudes were cut by subtraction. By subtracting from the amplitudes affected by caustic, the small amplitude variations were conserved. After the subtraction, all amplitudes where scaled between magnitude 1 and 2 using the rescale command in Matlab. This was done in order to enhance variations without sacrificing weak amplitudes.

The resulting seismograms proved very similar, but differences were found when subtracting the quintic traces from the cubic traces. The part of the seismograms where the differences were on their largest were isolated and enlarged in separate figures.

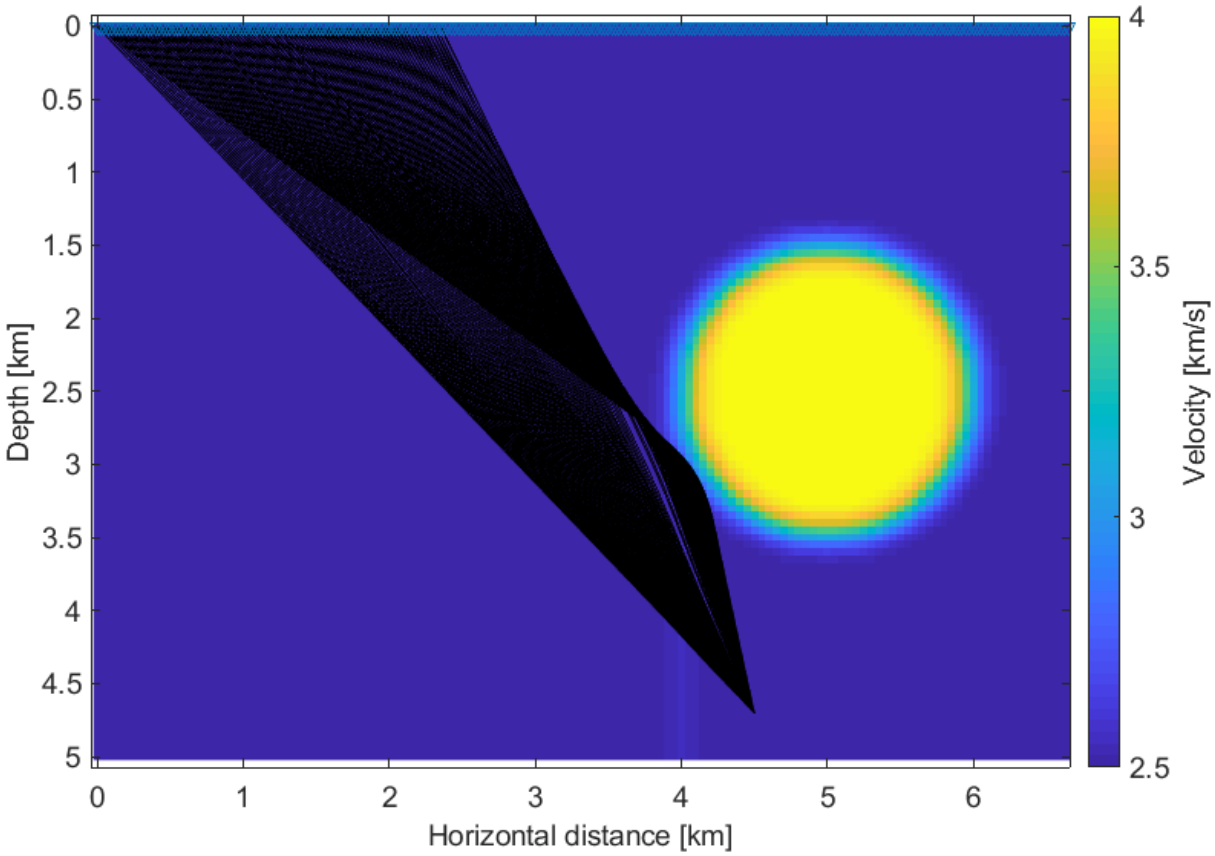

Figure 4.23: *Selected rays for seismograms*

The receivers selected to contribute to the seismograms were on the interval 0-2.35 km. These receivers were chosen because of the fold in the wavefield, see Figure 4.22. This selection ensured two arrivals for each trace.

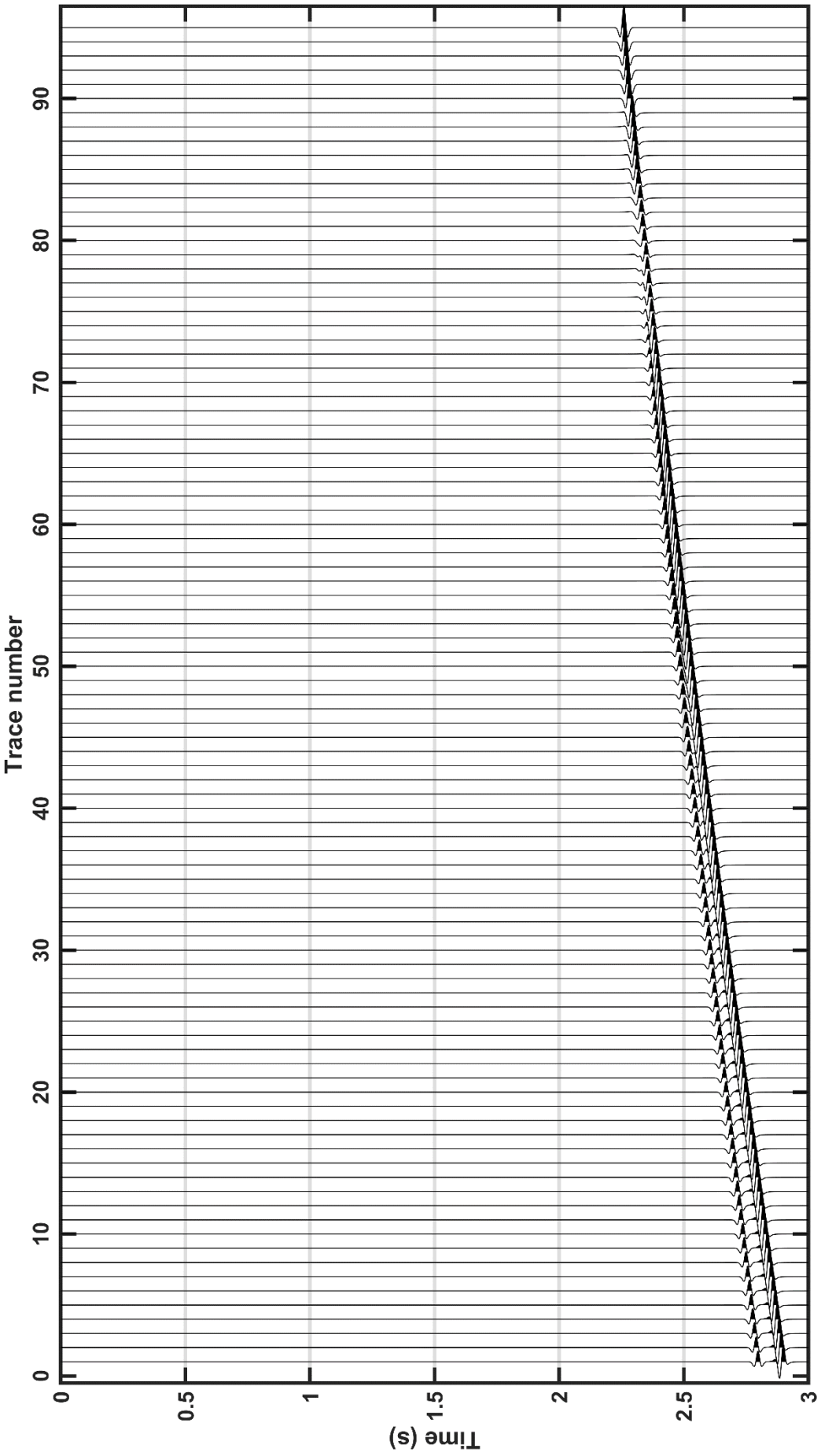

Figure 4.24: *Wiggle plot from the perturbed salt model using quintic spline representation.*

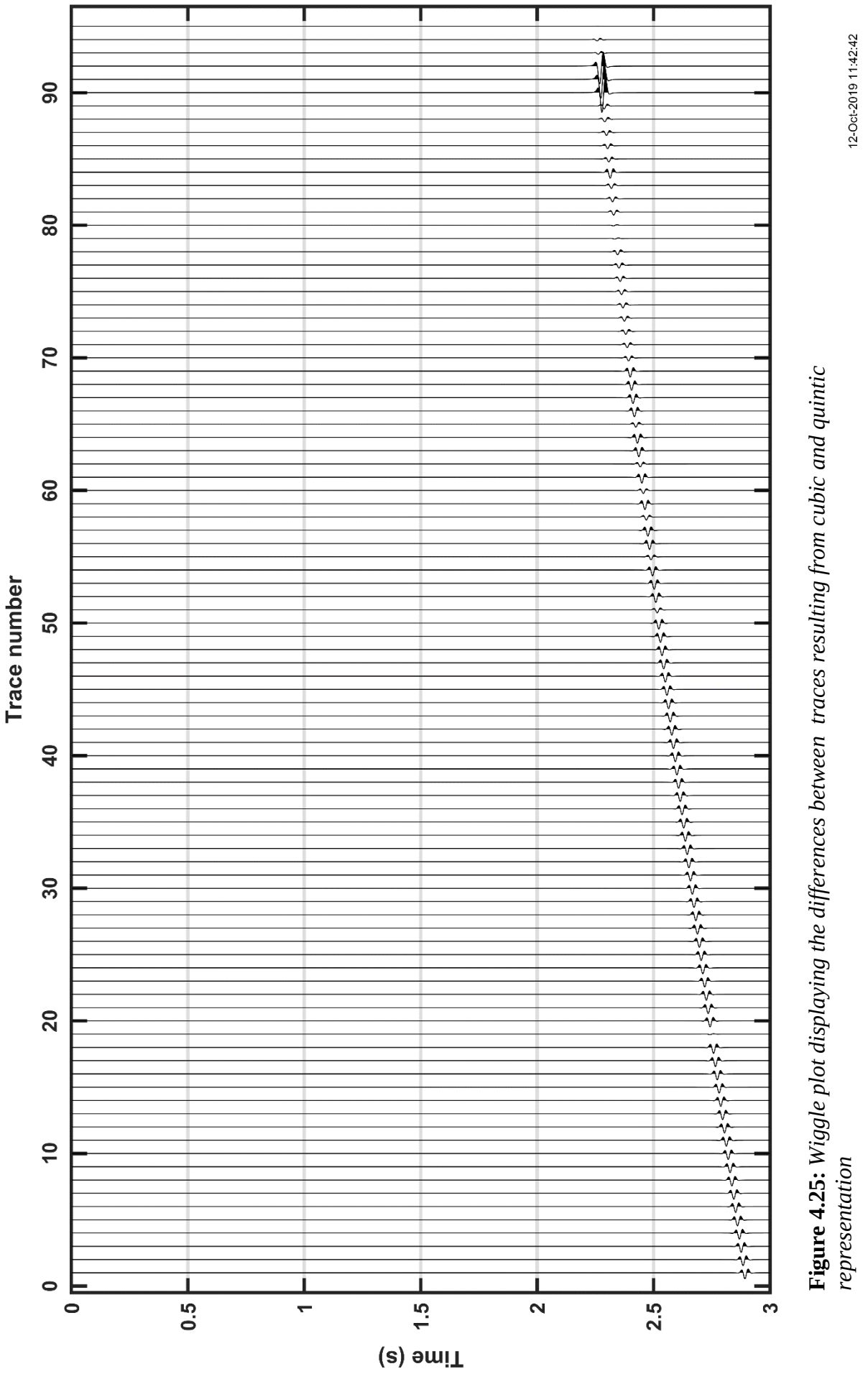

Figure 4.25: *Wiggle plot displaying the differences between traces resulting from cubic and quintic representation*

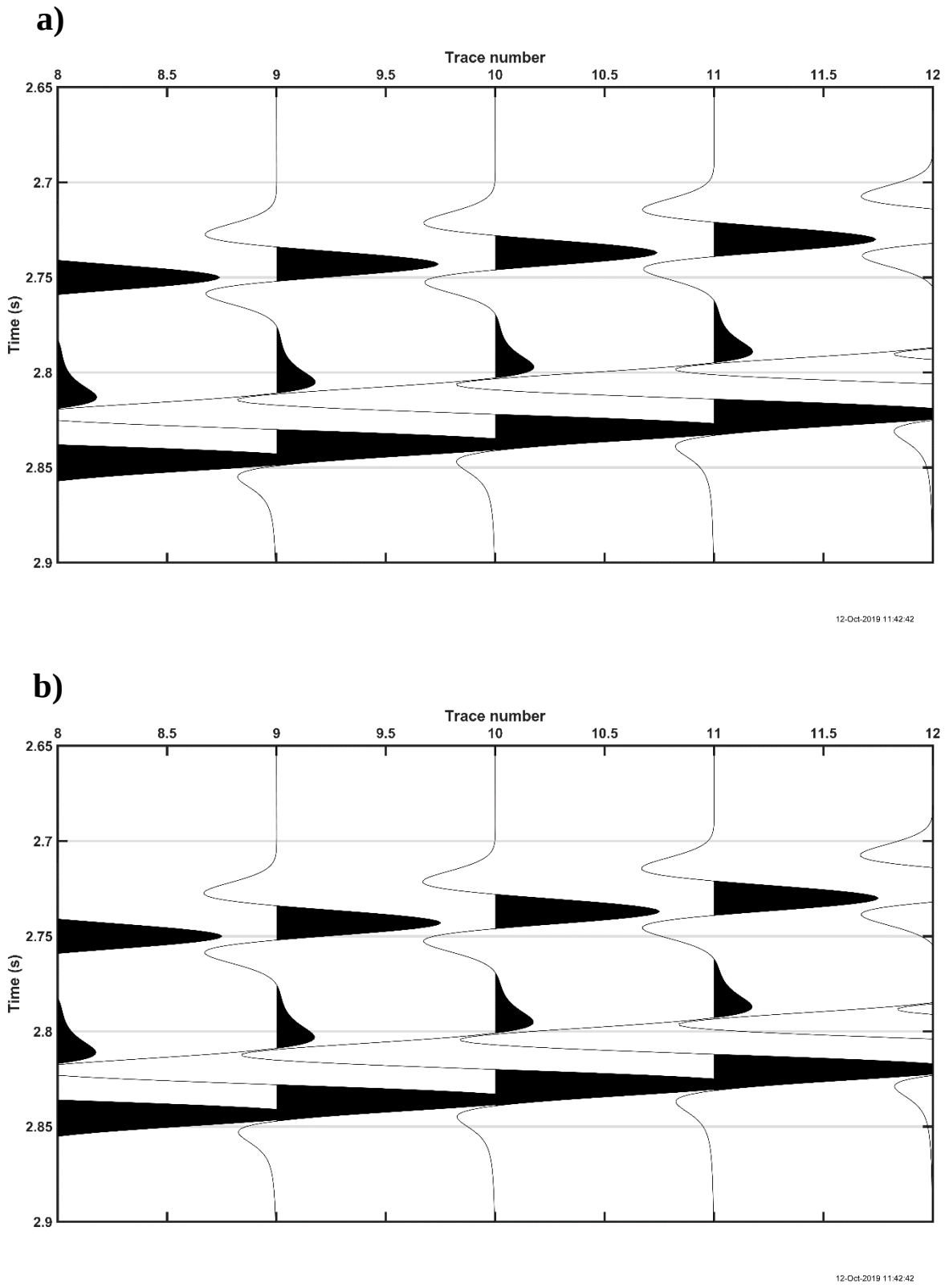

Figure 4.26: *Zoom in om traces 9-11 for a) the cubic representation and b) the quintic representation.*

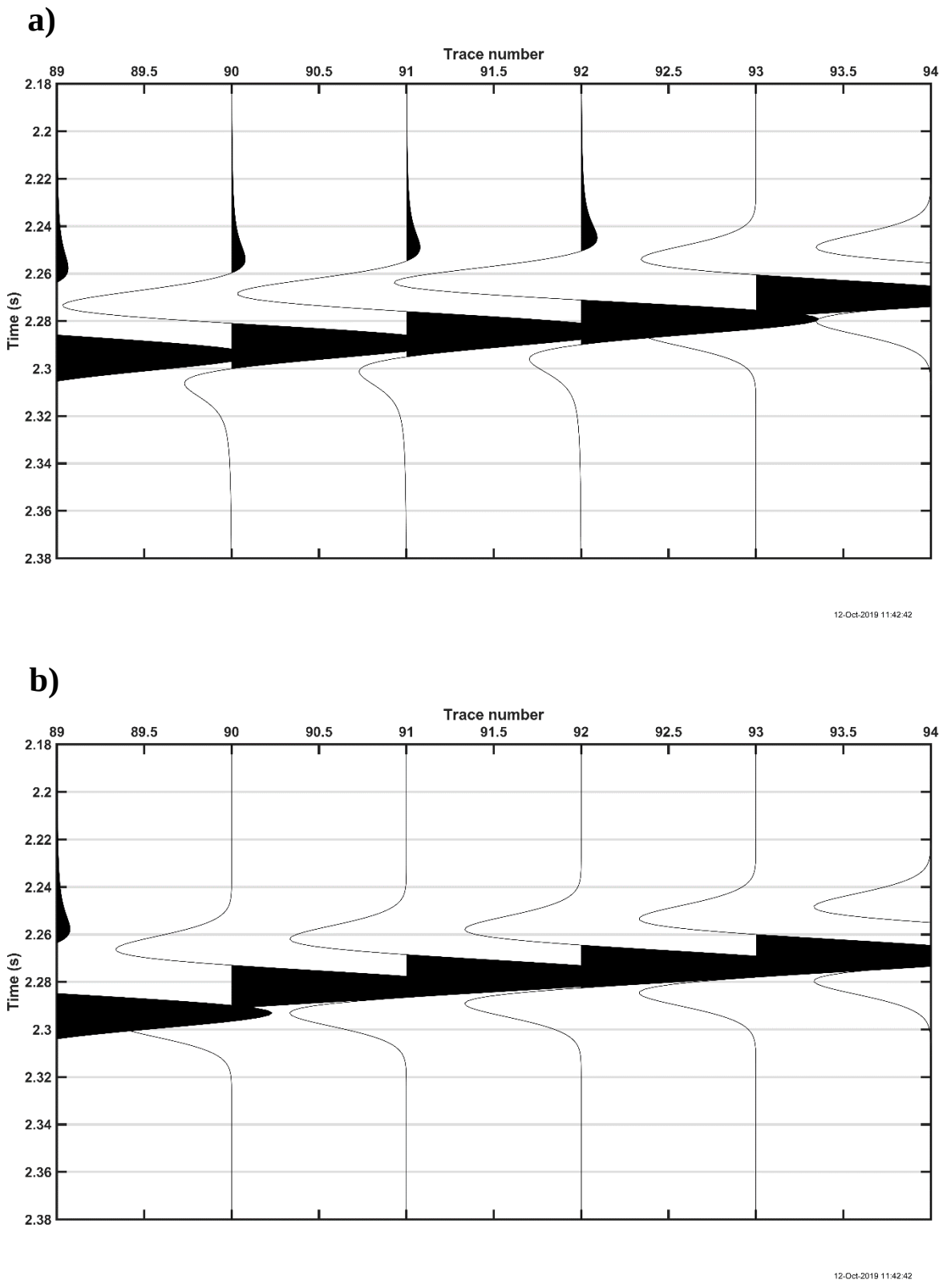

Figure 4.27: *Zoom in om traces 90-93 for a) the cubic representation and b) the quintic representation.*

As mentioned earlier, it was hard to distinguish between the seismograms for the cubic and the quintic representation. In Figure 4.26 it is possible to see that there is a difference in travel time for the second arrivals. In Figure 27, the difference in travel time can easily be spotted for traces 90-93, here we can also see that the amplitude for the cubic representation is sligthly larger than for the quintic representation. The means that the differences detected for these arrivals in Figure 4.25 can be caused by both a difference in amplitude and a small change in travel time. The differences in the first arrivals are to small to be detected or does not exist. Because of the simplicity of the salt model, the difference in the velocity representation is only located around the border area of the salt sphere, see section 4.3.2. This again leads to a small discrepancy in travel time between the cubic and quintic representation, though only for the second arrivals, which represent the rays in the fold (see the left part of Figure 4.22).

4.5 Extrapolation travel time

Extrapolation of travel time was done in the perturbed Marmousi model. The receiver distance for the true travel time was set to 25 metres. Because the second order travel time extrapolation was used, any large differences were not expected between the cubic and the quintic spline representation. The figure below shows the area of where the travel time extrapolation was performed. The ray marked in red represent the reference ray for the extrapolation.

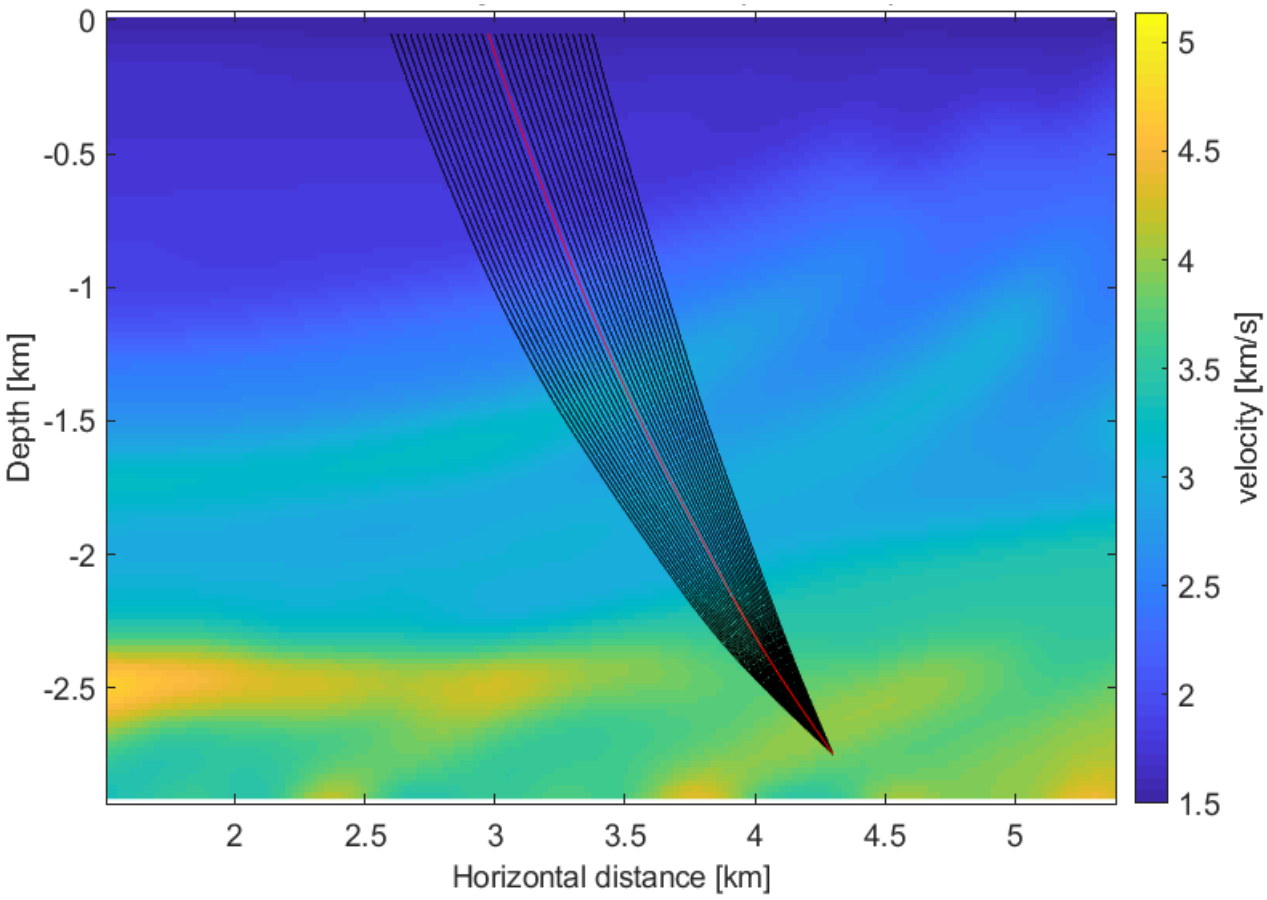

Figure 4.28: *Selected rays for extrapolation, the reference ray for the extrapolation is marked in red.*

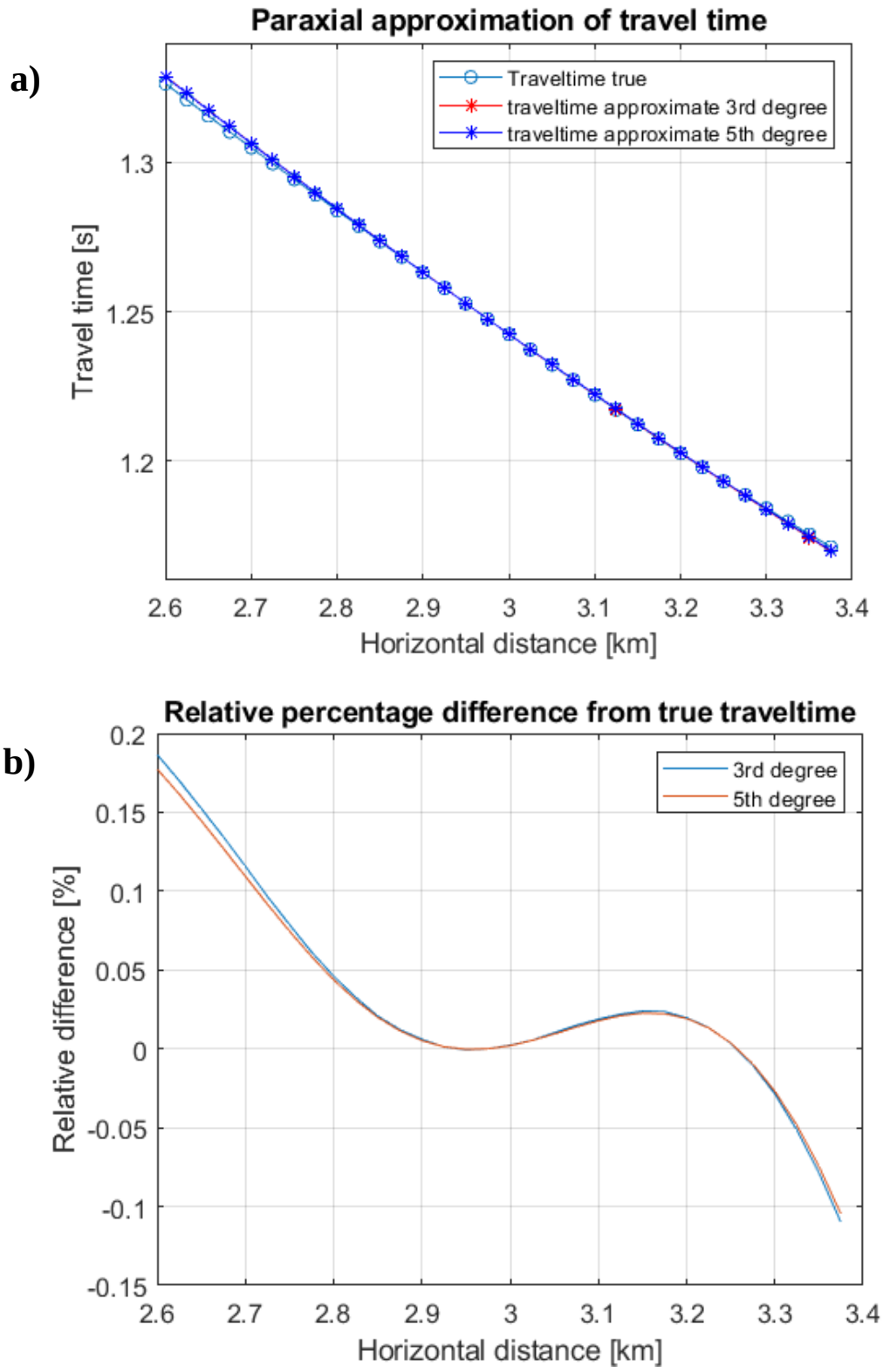

Figure 4.29: *a) the extrapolated travel time for cubic and quintic spline representation versus the true travel time. b) the relative difference from true travel time for the two different spline representations.*

As mentioned earlier, the second order extraction of travel time was not expected to reveal any major differences in the results. The quintic spline however, do have smooth second order derivatives, as opposed to the linearity of the second order derivatives of the cubic spline. This leads us to expect at least a tiny improvement of the exactness of the travel time extrapolation using the higher order spline representation.

Figure 4.27 a) reveals that the extrapolated travel time is very close to the true travel time for both the cubic and the quintic representation. Because of both the excessive smoothing done in the model, and the area chosen for the extrapolation, the true travel time curve is smooth and easier to estimate by extrapolation than it could have been in a “harder” model. Even though both the extrapolated travel time curves are close to the true travel time, Figure 4.27 b) reveals that the quintic representation is a bit closer over the whole extrapolated curve.

5 Discussion

In this thesis I have studied the differences in attributes for earth models with different continuity properties. The focus of the study was to test if the quintic spline representation could make ray tracing more robust for local variations in the velocity field. If so, the effect on the attribute computation also needs to be documented. Additionally, the study also set out to discover if the higher order spline would be worth the extra computation time. In this chapter I first discuss the effect the greater smoothness of the higher order spline (quintic) representation have on the ray path and velocity representation. Second, I discuss the how the different degree of continuity of the higher order spline affects the extrapolation of travel time.

5.1 Smoothness

As mentioned in section 2.3, the stiffness of a spline is related to the degree of polynomial function which it is expressed by. Model 0 ,see Figure 4.1, was smoothed to test the differences of the cubic and quintic spline methods with the intention to better understand the effects of using a higher order method. Figure 4.2, which illustrates smoothing after one iteration, is the most relevant illustration for this study. We can however get an idea of the efficacy of the use of quintic spline versus cubic spline, by running additional iterations. In section 3.4 it is illustrated how the higher order spline representation is dependent on more grid points for representing the value for a query point.

Figures 4.2 – 4.5 demonstrates how the higher degree spline smooths a model at a faster rate, elaborated in the graph in Figure 4.6. The models smoothed by the higher order spline more effectively approaches the mean value, using fewer iterations, than the models smoothed by the lower order spline. After one iteration of smoothing, illustrated in Figure 4.2, the sharp edges of model 0 have been rounded. The difference between the two methods are already visible. In a velocity model suited for ray tracing, there should not be such sharp transitions apparent in model 0. These results indicate that the higher order spline could be better suited for hard models, as opposed to the cubic spline. Though the performance relative to iterations was better, the computation time of the higher degree representation was not.

As shown in section 4.1, the computation time is significantly longer calculating quintic splines. Nearly all the calculations in the smoothing code, used on the models in section 4.1, were spline representations. The graph in Figure 4.7 compares the computation time relative to the number of iterations for the two spline methods. Since the number of query points are equal, Figure 4.7 is a good representation of the deviations in computation time between cubic and quintic spline representation. The difference in computation time was also quite noticeable in the ray tracer. When employing the quintic spline representation, the computation time was nearly doubled. One must take into account that these codes were mainly constructed to work and has not been optimized. The only difference between these B-spline calculations were the number of grid points used and the number of basic functions.

The continuity of the higher order derivatives is a motivation for studying the use of higher degree spline curves in ray tracing. Higher order dynamic ray tracing is used to obtain higher order derivatives of perturbations in position and slowness.

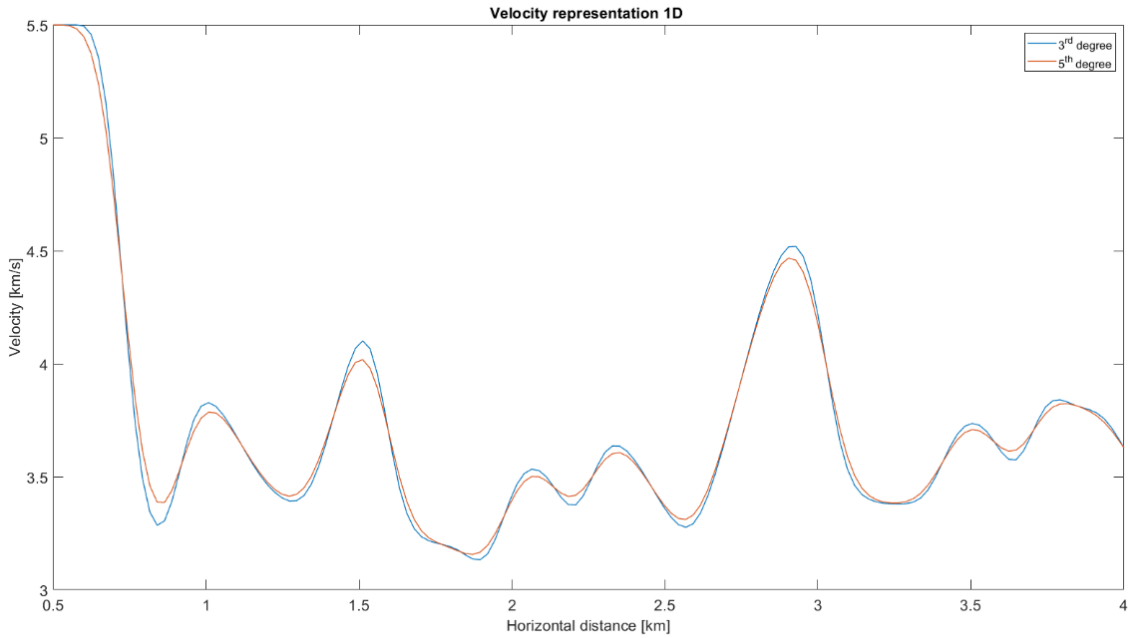

Figure 5.1: *A 1D velocity model extracted from the Marmousi model at, x=0-4.5 km, z=2.616 km. The velocity representation after one iteration are "stiffer" for the cubic representation (blue curve), than for the quintic representation (red curve).*

5.2 Ray tracing

The use of the higher order spline representation should produce a noticeable effect, considering the discussion from chapter 5.1, on both the robustness of the two-point ray tracer and attributes calculated from ray tracing.

5.2.1 Robustness

Since the quintic spline representation is smoother than the cubic representation, one hypothesis was that it would make the two-point ray tracing more efficient, meaning that Newton's method could use fewer iterations to reach the desired end point. A small perturbation in the takeoff angle at the source point can lead to a significant deviation in the ray path. In models like the Marmousi model, where there is a lot of detail, such a perturbation can have a drastic effect. When there is a higher degree of smoothing along the ray path, it appears that the perturbation of the takeoff angle would not cause the ray to deviate to far from the reference ray.
This hypothesis was tested in the Marmousi models, see section 4.2.1.

The hypothesis proved conclusive as the quintic spline representation presented a higher level of robustness. The anomaly used in the test where situated just above the source, to provide a certain stress aspect for the two-point ray tracing. Because the quintic representation requires more grid points in the model to represent the velocity function, the resulting velocity value will not be affected to as large degree as the cubic representation. In other words, the quintic spline representation provides greater smoothing along the ray than the cubic spline representation. In models with strong local velocity variation, the quintic representation will perform better, and provide a higher level of stability to the ray tracer.

5.2.2 Velocity representation and ray path

The reason for doing this study was to find out how the higher order spline affect the seismic attributes. As can be seen in Figure 5.1, the quintic spline representation is smoother and the norm of the represented values seems to be lower than the cubic spline. In section 4.3 the figures showed that there was a small difference in velocity between the two spline methods.

The direction of a ray at a fixed point in time is given, in isotropic media, directly by the slowness vector. The magnitude of the slowness vector equals the inverse wave velocity. The

velocity plots in section 4.3 illustrates that the difference in velocity is quite small. This slight difference causes the rays of the quintic method to deviate slightly from the ray path represented by cubic splines, as is also illustrated in section 4.3. The largest differences tend to occur around zones with considerable velocity variations.

For a smooth model, the variations in velocity representation (cubic versus quintic) are smaller than for a harder version of that same model. The use of a harder model could potentially produce significant deviations in ray path between the cubic and quintic spline representations. These results prove that even though the quintic representation do provide a greater smoothing along the ray, in smooth models, the differences between the cubic and quintic representation are relatively small.

5.2.1 Amplitudes

The results for the differences in amplitude stands out from the previous attributes calculated. In Figure 4.22 the relative difference between the amplitudes (cubic and quintic representation) is as much as 1.2, which means around 120 % difference.
The large differences that can be seen in the amplitude plots could be due to the perturbation of the ray path, which leads to a change in the position of caustics. Since the amplitudes increases drastically around the caustics, and the caustics are shifted due to the shift in ray path, the differences in amplitude will be large. In a caustic free zone, the amplitude differences are small.

In the figure below, Figure 5.2, the rays in a caustic free zone has been isolated to better study the amplitude differences. It can be seen that the relative difference is less than one percent. The rays presented in the figure are situated at the left side of the Marmousi model. All findings in this study suggests minimal discrepancies in attributes calculated using cubic and quintic spline. To further explore this, synthetic seismograms where made of the salt model, see section 4.4.1.

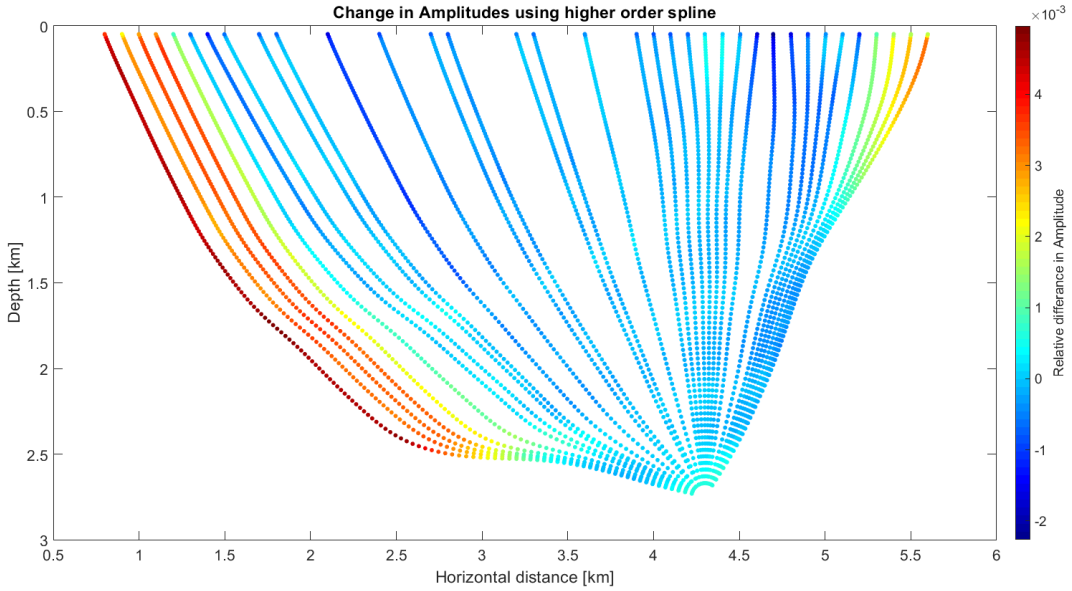

Figure 5.2: *Amplitude differences in in a caustic free zone. The relative difference in amplitudes between cubic and quintic spline representation, are small.*

The synthetic seismograms generated from the salt model proved very similar for the cubic and the quintic representation. In order to find any discrepancies, the traces from the quintic representation was subtracted from the traces for the cubic representation. The results revealed that there existed differences. In an attempt to decide the cause of the discrepancies, two parts of the seismograms were isolated and enlarged. From the traces in the enlarged zones, it was discovered a tiny shift in arrival time for some of the arrivals. Additional to this time shift, it was discovered that the amplitudes of the second arrivals for the cubic representation where larger than the same arrivals for the quintic representation. These arrivals represented rays that had been folded away from the salt sphere. Because the quintic spline provides greater smoothing along the ray, areas in the model where rays are focusing will in general become less prominent. This means that the ray tube for the quintic representation tends to be wider near caustics than for the cubic representation, which is the reason for the smaller amplitudes obtained using the quintic representation.

Calculation of travel time is dependent on the velocity. Because of the smoother representation of the quintic spline, see Figure 5.1, the represented velocities in a heterogeneous medium will be different from the cubic spline. This difference in velocity representation is bound to have an effect on the travel time. The models used in this thesis are

smoothed to a high degree before raytracing is done, so that the travel time is not affected in as high a degree as it could have been. A model with stronger local variation, should produce a more noticeable shift in the calculated travel times.

5.3 Higher order derivatives

As mentioned in the introduction, an additional motivation for this thesis is the need for higher order derivatives in the study of paraxial extrapolation. In the past few years, the interest in higher order extrapolation of seismic attributes has increased, see Iversen et al. (2019). Even though the extrapolation done in this thesis is only to the second order, it is important to mention how the quintic spline representation opens for more possibilities in paraxial extrapolation.

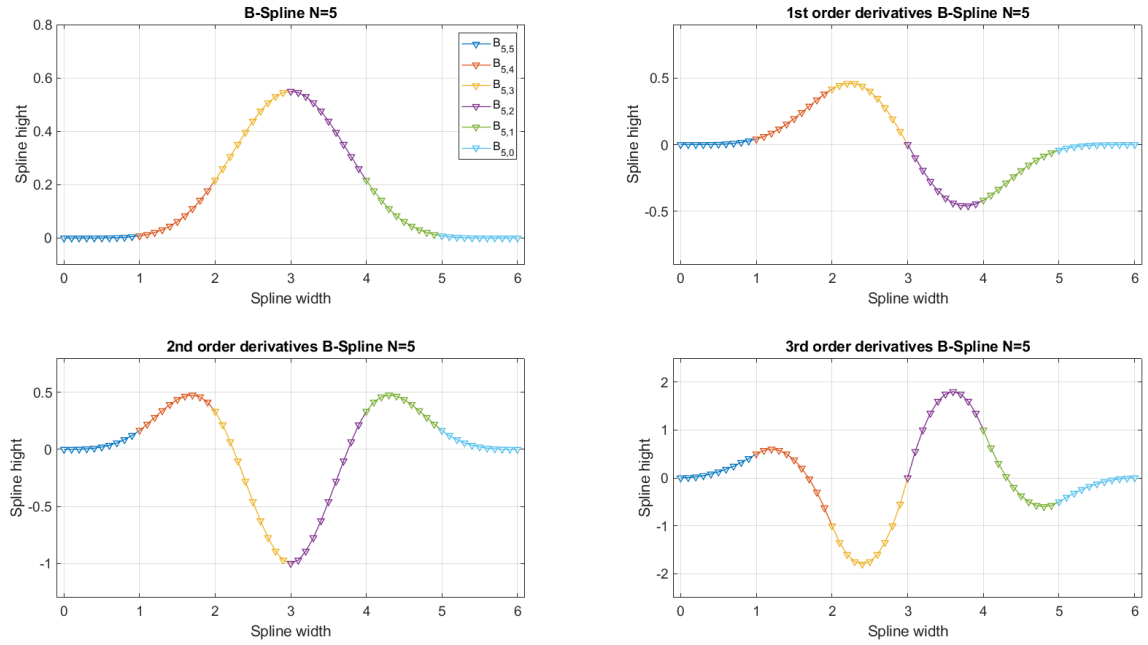

Figure 5.3: *Illustration of a quintic B-spline curve and its derivatives up to third order.*

The quintic spline has continuity C^4, which means that it has continuous derivatives up to fourth order. The figure above, Figure 5.3, illustrates a quintic B-spline curve and its derivatives up to third order. One can observe that the higher order derivatives are smooth and stable. In the context of ray tracing, this means we have access to stable derivatives of the velocity up to at least third order, as the fourth order derivatives will be linear.

The second order travel time extrapolation in section 4.5 demonstrates the effect that smooth derivatives have on the estimated travel time curve. As can be seen from the figures, the estimated travel time for the quintic representation is slightly closer to the true travel time. This may be due to the smoother second order derivatives.

The plot in Figure 5.4 illustrates how the derivatives of a 1D velocity line looks like with both the quintic and cubic spline representations. Here we can see clearly the difference between the derivatives, and the smoothness of the second order derivatives of the quintic spline representation. It is easy to see that the use of a quintic representation should have an effect on the extrapolation of travel time. The second order derivatives for the cubic representation are piecewise linear functions.

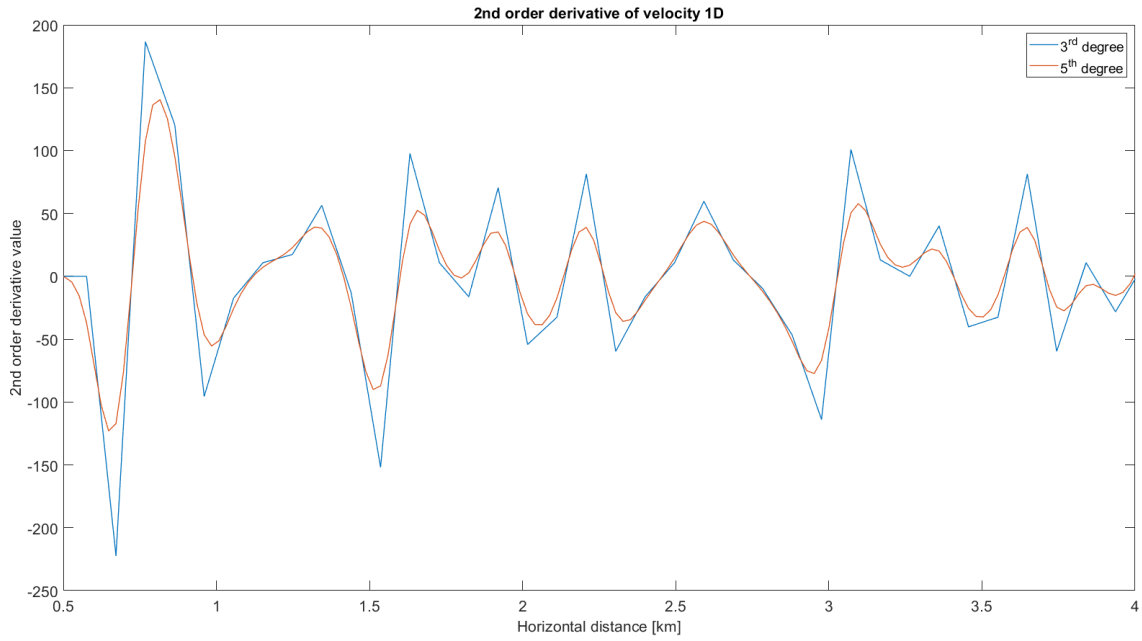

Figure 5.4: *Comparison of the cubic and quintic second order derivatives of a 1D velocity function.*

For higher order extrapolation of travel time, we need higher order derivatives of travel time. These can be found by higher order Hamilton-Jacobi perturbation equations (Iversen et al., 2019), or without (Červený, 2001, Klimeš, 2002, Klimeš, 2006, Goldin and Duchkov, 2003). The higher order Hamilton-Jacobi perturbation equation are dependent on the higher order derivatives of the velocity field. This means that for extrapolation of travel time of higher order than two, there need to be continuous derivatives of the velocity field higher than

second order. The quintic spline provides continuous derivatives up to fourth order, which provides the possibility of travel time extrapolation of fourth order.

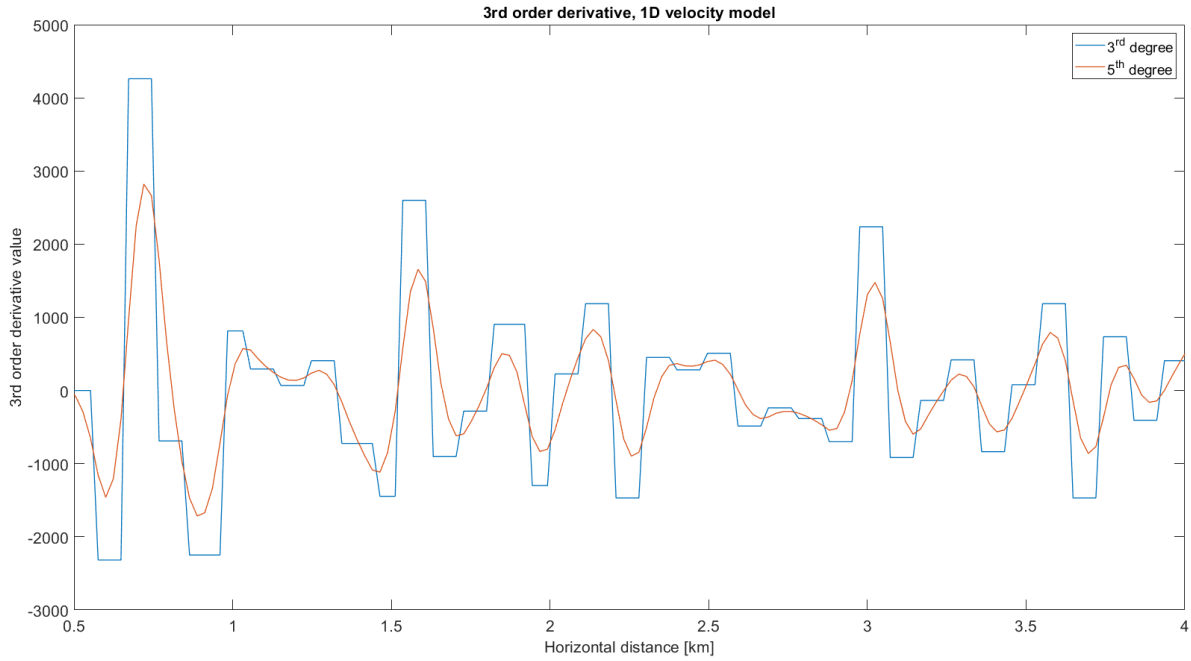

Figure 5.5: *Comparison of the cubic and quintic third order derivatives of a 1D velocity function.*

Figure 5.5 demonstrates the different degree of continuity of the cubic and the quintic spline. Here, the third order derivatives of the 1D velocity function from Figure 5.1 is displayed for both the cubic and the quintic spline representation.

6 Conclusion

The objective of this work has been to study the effect of using higher-order splines in the modelling of seismic attributes.

My main conclusion is that a quintic spline representation yields a considerably higher degree of robustness for two-point ray tracing. I demonstrated this for different test cases including strong local velocity variation.

I note that the difference in ray path and velocity (along the ray) is quite small and is not affected to great extent when employing the quintic spline representation rather than cubic spline representation. There is, however, a significant difference in amplitudes due to the small change of the ray path. Because the magnitude of the amplitude increases drastically near caustics, even a small shift in the position of the caustic (shift in the ray path), results in a severe difference in amplitude. For caustic-free parts of the ray field I observe that the two representations yield almost equal results, for travel time as well as amplitude.

The smoothing ability of the quintic spline is considerably better than for the cubic spline. As the grid points of the model are invariant, the quintic spline also provides greater smoothing along the ray.

The need for pre-smoothing of a model (prior to ray tracing) decreases to some extent by using the quintic B-spline representation, although it is unrealistic to think that this type of smoothing can be replaced completely by the model representation method.

The computation time of direct ray tracing is clearly higher for the quintic than for the cubic spline representation method. For two-point ray tracing this difference is somewhat moderated, since two-point ray tracing with the quintic spline representation requires a smaller number of iterations. Nevertheless, when discussing computation times, it is important to keep in mind the enormous increase of computational capacity that has taken place since the 1970s, when the cubic B-spline was introduced in seismic modelling. In this perspective, I believe we can afford in 2019 to utilize a somewhat more time-consuming method to represent the geological model.

For further work I suggest:

- To employ the quintic spline representation for an anisotropic medium, as this is often a more realistic medium, compared to the isotropic case.
- To test the quintic spline representation method in a model with interfaces. As is already shown in this thesis, there is a slight difference in the represented velocities, which may be accentuated by the use of Snell's law at the interfaces.
- To optimize the codes, for better computational performance.
- To push the quintic spline representation to its limits, by introducing rougher models.

7 References

ADAMS, R. A. & ESSEX, C. 2013. *Calculus: a complete course,* Toronto, Pearson.

BORTFELD, R. 1989. Geometrical ray theory: Rays and traveltimes in seismic systems (second-order approximations of the traveltimes). *Geophysics,* 54**,** 342-349.

CARCIONE, J. M., HERMAN, G. C. & TEN KROODE, A. P. E. 2002. Seismic modeling. *Geophysics,* 67**,** 1304-1325.

ČERVENÝ, V. 1972. Seismic Rays and Ray Intensities in Inhomogeneous Anisotropic Media. *Geophysical Journal of the Royal Astronomical Society,* 29**,** 1-13.

ČERVENÝ, V. 2001. *Seismic ray theory,* Cambridge, Cambridge University Press.

ČERVENÝ, V. & HRON, F. 1980. Ray series method and dynamic ray tracing system for 3-dimetional inhomogeneous media. *Bulletin of the Seismological Society of America***,** 47-77.

ČERVENÝ, V., IVERSEN, E. & PŠENČÍK, I. 2012. Two-point paraxial traveltimes in an inhomogeneous anisotropic medium. *Geophysical Journal International***,** 1597-1610.

ČERVENÝ, V., KLIMEŠ, L. & PŠENČÍK, I. 1988. Applications of dynamic ray tracing. *Physics of the Earth and Planetary Interiors,* 51**,** 25-35.

ČERVENÝ, V., MOLOTKOV, I. A. & PŠENČÍK, I. 1977. *Ray method in seismology*, Univerzita Karlova.

ČERVENÝ, V., POPOV, M. M. & PŠENČÍK, I. 1982. Computation of wave fields in inhomogeneous media — Gaussian beam approach. *Geophysical Journal of the Royal Astronomical Society,* 70**,** 109-128.

CHANG, G. & SEDERBERG, T. W. 1997. Bézier Curves. *Over and Over Again.* Washington, D.C.: Mathematical Association of America.

DE BOOR, C. 1978. *A practical guide to splines,* New York, Springer Verlag.

DE BOOR, C. 1993. B-Spline Basics. *Fundamental Developments of Computer-Aided Geometric Modeling.* Academic Press.

DRUMMOND, R. 1982. Body-wave seismograms in inhomogeneous media using Maslov asymptotic theory. *The Bulletin of the Seismological Society of America BSSA,* 72**,** S277-S317.

FARIN, G. E., HOSCHEK, J. & KIM, M.-S. 2002. *Handbook of computer aided geometric design*, Elsevier.

FARRA, V. & MADARIAGA, R. 1987. Seismic waveform modeling in heterogeneous media by ray perturbation theory. *Journal of Geophysical Research: Solid Earth,* 92**,** 2697-2712.

GJØYSTDAL, H., IVERSEN, E., LAURAIN, R., LECOMTE, I., VINJE, V. & ASTEBØL, K. 2002. Review of ray theory applications in modelling and imaging of seismic data. *Studia Geophysica et Geodaetica,* 46**,** 113-164.

GJØYSTDAL, H., IVERSEN, E., LECOMTE, I., KASCHWICH, T., DROTTNING, A. & MISPEL, J. 2007. Improved applicability of ray tracing in seismic acquisition, imaging, and interpretation. *Geophysics,* 72**,** 261-271.

GOLDIN, S. V. & DUCHKOV, A. A. 2003. Seismic Wave Field in the Vicinity of Caustics and Higher-Order Travel Time Derivatives. *Studia Geophysica et Geodaetica,* 47**,** 521-544.

IVERSEN, E., URSIN, B., SAKSALA, T., ILMAVIRTA, J. & DE HOOP, M. V. 2019. Higher-order Hamilton–Jacobi perturbation theory for anisotropic heterogeneous media: dynamic ray tracing in Cartesian coordinates. *Geophysical Journal International***,** 2044-2070.

KEERS, H., DAHLEN, F. A. & NOLET, G. 1997. Chaotic ray behaviour in regional seismology. *Geophysical Journal International,* 131**,** 361-380.

KEHO, T. H., BEYDOUN, W. B. & KEHO, T. H. 1987. The paraxial ray method. *Geophysics,* 52**,** 1639-1653.

KLIMEŠ, L. 2002. Second-order and higher-order perturbations of travel time in isotropic and anisotropic media. *Studia Geophysica et Geodaetica,* 46**,** 213-248.

KLIMEŠ, L. 2006. Spatial derivatives and perturbation derivatives of amplitude in isotropic and anisotropic media. *Studia Geophysica et Geodaetica,* 50**,** 417-430.

KREBES, E. S. 2004. Seismic Forward Modeling. *CSEG Recorder 30***,** 28-39.

LECOMTE, I., LAVADERA, P., ANELL, I., BUCKLEY, S. J., SCHMID, D. & HEEREMANS, M. 2015. Ray-based seismic modeling of geologic models: Understanding and analyzing seismic images efficiently. *Interpretation,* 3**,** SAC71-SAC89.

MUSSETT, A. E. & KHAN, M. A. 2000. *Looking into the earth: an introduction to geological geophysics,* Cambridge, Cambridge University Press.

NOWAK, G. 2011. A de Casteljau Algorithm for -Bernstein-Stancu Polynomials. *Abstract and Applied Analysis,* 2011.

PRIIMENKO, V. & MITROFANOV, G. 2018. KMAH index and separation of PSP-waves from streamer data.

SAUER, T. 2012. *Numerical analysis,* Boston, Mass, Pearson.

USHAKOV, D. 2011. *NURBS and CAD: 30 years together* [Online]. Isicad. Available: http://isicad.net/articles.php?article_num=14940 [Accessed 14/10 2019].

ZHDANOV, M. S., LEE, S. K. & YOSHIOKA, K. 2006. Integral equation method for 3D modeling of electromagnetic fields in complex structures with inhomogeneous background conductivity. *Geophysics,* 71**,** G333-G345.

Appendix A: Cubic and Quintic B-spline basis functions

The following equations are basis functions for third (cubic) and fifth (quintic) degree basic splines, derived from the de Boor algorithm.

Cubic spline basis functions:

$$b_{3,0} = \frac{1}{6}(-t^3 + 3t^2 - 3t + 1)$$

$$b_{3,1} = \frac{1}{6}(3t^3 - 6t^2 + 4)$$

$$b_{3,2} = \frac{1}{6}(-3t^3 + 3t^2 + 3t + 1)$$

$$b_{3,3} = \frac{1}{6}t^3$$

Quintic spline basis functions:

$$b_{5,0} = \frac{1}{120}(-t^5 + 5t^4 - 10t^3 + 10t^2 - 5t + 1)$$

$$b_{5,1} = \frac{1}{120}(5t^5 - 20t^4 + 20t^3 + 20t^2 - 50t + 26)$$

$$b_{5,2} = \frac{1}{120}(-10t^5 + 30t^4 - 60t^2 + 66)$$

$$b_{5,3} = \frac{1}{120}(10t^5 - 20t^4 - 20t^3 + 20t^2 + 50t + 26)$$

$$b_{5,4} = \frac{1}{120}(-5t^5 + 5t^4 + 10t^3 + 10t^2 + 5t + 1)$$

$$b_{5,0} = \frac{1}{120}t^5$$